ISSN 0280-5316
ISRN LUTFD2/TFRT--5831--SE

ESP for Suppression of Jackknifing in an Articulated Bus

Karl Berntorp

Department of Automatic Control
Lund University
December 2008

Lund University
Department of Automatic Control
Box 118
SE-221 00 Lund Sweden

Document name
MASTER THESIS

Date of issue
December 2008

Document Number
ISRN LUTFD2/TFRT--5831--SE

Author(s)
Karl Berntorp

Supervisor
Daniel Keppler and Jens Kalkkül at Daimler AG, Germany
Karl-Erik Årzén Automatic Control, Lund (Examiner)

Sponsoring organization

Title and subtitle
ESP for Suppression of Jackknifing in an Articulated Bus (ESP för motverkan av fällknivseffekten i ledbussar)

Abstract
The Electronic Stability Program (ESP) is becoming increasingly popular in vehicles as a means to prevent spin-out and lane departure accidents, and is nowadays a standard feature in most cars. From 2012 the ESP will also be a standard feature in buses. As a first step, this thesis is dedicated to implementing an ESP for an articulated bus in simulation using Matlab/Simulink. The core of the ESP is a yaw rate controller that calculates a moment about the center of gravity of the front part of the bus to stabilize it. Integrated in the ESP are also an Anti-lock Braking System (ABS) and an Anti-Spin Regulation (ASR) system, which are model-based controllers that produce the brake pressures needed to achieve the desired moment. For the articulated bus it is clear that the fact that the bus consists of two parts makes the problem of stabilizing the bus more difficult. Furthermore, for articulated vehicles it is known
that the risk of having the vehicle folding, known as jackknifing, during cornering is a major problem. However, the ESP is found to stabilize the bus for a large number of maneuvers and loading configurations, as well as suppressing jackknifing.

Keywords

Classification system and/or index terms (if any)

Supplementary bibliographical information

ISSN and key title
0280-5316

ISBN

Language
English

Number of pages
84

Recipient's notes

Security classification

Contents

Acknowledgments . . . 3

1. Introduction . . . 4
- 1.1 Background . . . 4
- 1.2 Motivation . . . 4
- 1.3 Tasks . . . 5
- 1.4 Outline . . . 5
- 1.5 Methods . . . 6
- 1.6 Limitations and Assumptions . . . 6
- 1.7 Miscellaneous . . . 6

2. Modeling . . . 7
- 2.1 Slip . . . 7
- 2.2 Tire Models . . . 8
- 2.3 Wheel Modeling . . . 11
- 2.4 Load Distribution . . . 13
- 2.5 Chassis Models . . . 15
- 2.6 Summary . . . 24

3. Slip Control Design . . . 25
- 3.1 ABS . . . 25
- 3.2 ASR . . . 32
- 3.3 Summary . . . 32

4. Evaluation of the Slip Control . . . 33
- 4.1 Evaluation of the ABS . . . 33
- 4.2 Discussion . . . 37
- 4.3 Evaluation of the ASR . . . 37
- 4.4 Discussion . . . 39

5. Yaw Rate Control Design . . . 40
- 5.1 Upper Controller . . . 40
- 5.2 Lower Controller . . . 47
- 5.3 Summary . . . 50

6. Evaluation of the ESP . . . 51
- 6.1 Stability Conditions . . . 51
- 6.2 Test Maneuvers . . . 52
- 6.3 Simulation Results . . . 54
- 6.4 Discussion . . . 68
- 6.5 Stabilization at Low Velocities . . . 69

7. Conclusions and Future Work . . . 72
- 7.1 Conclusions . . . 72
- 7.2 Future Work . . . 72

8. Bibliography . . . 73

A. Nomenclature and Definitions . . . 75
- A.1 Abbreviations . . . 75
- A.2 Symbol Descriptions . . . 75
- A.3 Mathematical Definitions . . . 77

B. Additional Plots . . . 79
- B.1 ABS Plots . . . 79

Acknowledgments

The work leading up to this report was performed between June and November 2008 at Daimler's Vehicle Dynamics Group GR/EAV in Sindelfingen, Germany. I would like to thank Prof. Karl-Erik Årzén in Lund for giving me the opportunity and coming up with the idea of doing the thesis at Daimler. Naturally, I would like to thank all at Daimler for making my stay in Germany a pleasant one. There are some who deserve special mentioning: First, my recognition goes to Dr. Jens Kalkkühl at Daimler for his approval of having me working at Daimler. I owe gratitude to Mr. Dennis Steffen for always having time to answer my questions about the simulation environment. Finally, I appreciate the assistance of my advisor, Mr. Daniel Keppler, throughout the project.

Karl Berntorp

1. Introduction

1.1 Background

Daimler AG produces different types of buses for commercial purposes. Among them are the linked buses, see Figure 1.1. Because the link is soft there is a risk that the

Figure 1.1 The Mercedes-Benz Citaro G

bus folds[1], for example during heavy cornering. The risk of jackknifing is normally greater the faster the bus travels, but it may also be a concern at low speed.

The trend in the automotive industry is to incorporate more and more driver assistance control systems into the vehicles, for example anti-lock braking systems preventing the wheels from locking during braking and traction control systems hindering the wheels from spinning when accelerating.

From 2012 the Electronic Stability Program (ESP) will be mandatory on buses with the purpose of preventing spin-out[2], lane departure and to some extent rollover accidents. This thesis investigates whether the ESP can be employed not just to prevent spin-out, but also to suppress jackknifing. It is possible that these two effects are dependent of each other, since it seems likely that the risk of jackknifing is increased if the bus is spinning, and vice versa.

1.2 Motivation

The first attempts of safety enhancement systems in vehicles were done in the 1920's. In the USA the first patent for anti-lock brakes was issued 1936, and the intention was to improve safety for aircraft landing. The first electronic ABS[3] for cars was introduced in 1978 [Burton *et al.*, 2004]. The ESP, which governs the stability of the whole system rather than certain components, is built on top of an anti-lock braking system and an anti-spin regulation system (ASR). A short description of the ESP and its components follows below.

The goal of an ABS is to make sure that the wheels do not lock during braking, and there are two reasons for this. One reason is that the maximum braking force that can be achieved is most often not reached when the wheels are locked, therefore leading to increased stopping distance. The second reason is that the lateral forces

[1] Also known as jackknifing.

[2] Spin-out is when the vehicle is spinning around its vertical axis.

[3] Anti-lock Braking System

of the wheels are greatly reduced when the wheels lock, making it a hard task for the driver to try to steer the vehicle. By controlling the brake pressure so that the maximum force is achieved, the brake distance can be minimized while keeping the vehicle steerable. Since the introduction of the ESP the ABS is not only required to prevent wheel lock, but also to achieve arbitrary brake forces.

The functioning of an ASR system is similar to that of an ABS. The goal is to make sure that the wheels do not spin during acceleration. This can, for example, be a problem when trying to accelerate on snow or ice or when going from a dry to wet surface. The reason for not wanting the wheels to spin is to maintain steerability of the vehicle.

Vehicle stability control systems that try to force the vehicle to follow a yaw rate[4] reference trajectory during extreme cornering, often referred to as Electronic Stability Programs, were first introduced in commercial vehicles in 1995 in Mercedes-Benz S-Class cars [Liebemann *et al.*, 2005]. The goal of an ESP is to prevent the vehicle from skidding by detecting loss of steerability and reacting appropriately. Skidding can be a concern, for example, during emergency turning or poorly judged curvature radius. As an example, assume a situation where the driver of a vehicle enters a curve at a too high speed. The vehicle may then start to skid, and as a result steerability can be lost, possibly leading to a crash. This is sensed by the ESP because of the difference between an estimated driver-desired yaw rate and the measured yaw rate. A possible interaction by the ESP is to demand the ABS to brake appropriate wheels to try to keep the motion of the vehicle stable. The brakes are, however, not the only feasible actuators in an ESP. Another possibility is to use the steering angle of the wheels to correct the driver's steering angle input.

Numerous studies have been conducted to show the importance of ESP. Studies in Sweden during the years 1998-2004 showed that ESP had an effectiveness on fatal crashes of around 50 percent. It was estimated that of the total 500 vehicle related deaths annually, up to 100 of them could have been avoided had the vehicles been equipped with an ESP. Also, a National Highway for Traffic Safety Administration (NHTSA) report in the USA showed a reduction of single vehicle crashes with 35 percent [Lie *et al.*, 2005]. There have also been investigations concerning the ESP's ability to prevent jackknifing of heavy articulated vehicles, something which will be discussed much more later.

1.3 Tasks

The tasks of this thesis are the following:

- Implement an ESP in simulation.
- Find critical maneuvers that makes the bus unstable.
- Investigate to what extent the ESP can prevent spin-out and suppress jackknifing.

1.4 Outline

The outline of the thesis is as follows: Chapter 2 deals with vehicle modeling, where tire models as well as chassis models are considered. Chapter 3 designs control al-

[4] Rotation velocity around the vertical axis of the center of mass.

gorithms for the ABS and the ASR. In Chapter 4 the developed controllers are evaluated. Chapter 5 designs the yaw rate controller that constitutes the last part of the ESP, which is evaluated in Chapter 6.

1.5 Methods

The tool used for system building in this thesis is Matlab/Simulink. For simulation, Daimler's CASCaDE[5] was used. CASCaDE is a very detailed simulator with correct suspension and force models and full degree of freedom chassis models, and hence the simulation results are very alike to those that would be produced in a real vehicle. It was used throughout the work to verify theory, finding critical maneuvers and tuning the controllers used.

1.6 Limitations and Assumptions

All states of the vehicle, for example velocities, are considered known unless stated otherwise. In a real environment these states are estimated using observers and sensors. The forces and loading conditions of the bus are considered unknown, since they are not available in a commercial vehicle. One of the most important variables in vehicle modeling is the coefficient of friction. This is also considered unknown.

1.7 Miscellaneous

Some notations used:

- Both scalars and vectors are denoted with small italic letters, for example x. It will hopefully be clear from the context what it should be interpreted as.
- The wheels are numbered from left to right, starting with the front axle.
- The front part of the bus will be referred to as tractor, and the rear part will be denoted trailer.
- The Euclidian norm of the vector x is written as $||x||$.
- The set of real numbers is $\mathbf{R}$.

The most common symbols used in the thesis are listed in Section A.2. Most mathematical definitions and theorems are stated as the text proceeds. However, some definitions are found in Section A.3 in order not to clutter the text more than necessary.

[5] Computer Aided Simulation of Car, Driver and Environment

2. Modeling

This chapter discusses different aspects of vehicle modeling and explains some different models. For in-depth reading about vehicle dynamics, the reader may benefit from [Kiencke and Nielsen, 2005], [Isermann, 2006] and [Schindler, 2007].

2.1 Slip

A quantity known as *slip* plays an important part in this thesis, which is because slip is the main reason why forces are generated between the tires and the road. There are many different kinds of slip, but only three of them will be reviewed here.

When the driver brakes or accelerates, longitudinal slip develops. In [Schindler, 2007] this is defined as

$$\lambda = \frac{v_{wx} - r\omega}{v_{wx}} = 1 - \frac{r\omega}{v_{wx}} \tag{2.1}$$

when braking and

$$\lambda = \frac{v_{wx} - r\omega}{r\omega} = \frac{v_{wx}}{r\omega} - 1 \tag{2.2}$$

when accelerating. Here, v_{wx} is the component of the wheel velocity in the longitudinal direction of the wheel and ω is the angular velocity of the wheel. r is the wheel's effective radius, that is the distance from the center of the wheel to the road. The normalization ensures that the slip is between -1 and 1.

The lateral slip angle is conventionally defined as

$$\tan\alpha = -\frac{v_{wy}}{v_{wx}}, \tag{2.3}$$

where v_{wx} and v_{wy} is the longitudinal and lateral wheel velocity, respectively. Figure 2.1 should clarify the situation. A convenient approach is to define lateral slip as $\sin\alpha$. The definition ensures that also this quantity is between -1 and 1. The third

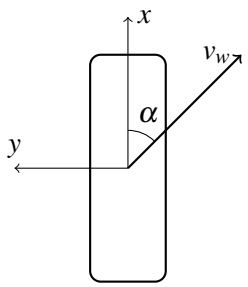

Figure 2.1 The wheel together with its coordinate system seen from above.

slip quantity considered in this thesis is the vehicle body sideslip angle β, which is defined through the vehicle's longitudinal and lateral velocity as

$$\tan\beta = \frac{v_y}{v_x}. \tag{2.4}$$

2.2 Tire Models

It is the contact between the tires and the road surface that generates the forces needed to alter the vehicle's speed and course. It is hard to come up with detailed models of the tires since they have a complex structure and depend on many things. Still, one can come pretty far by using quite simple empirical approaches. Some of these are reviewed in this section.

The tire forces can be split up into its longitudinal and lateral part, respectively. Both forces depend on several inputs, being λ, α, the coefficient of friction μ between the tire and the road, the normal force F_z acting on the wheel and the angle between the vertical axis of the road and the wheel, among others.

Pacejka Formula

One empirical approach used to model the forces is the *Pacejka Formula* [Klěcka, 2007]. It is given by

$$y(x) = D\sin\Big(C\arctan\big(Bx - E(Bx - \arctan(Bx))\big)\Big),$$

where

B is the stiffness factor

C is the shape factor

D is the peak factor

E is the curvature factor

y is either the longitudinal or the lateral force, and x is either λ or α. The typical curve that is generated by this formula, shown in Figure 2.2, is very close to experimental results when only one of longitudinal and lateral slip occurs at the same time.

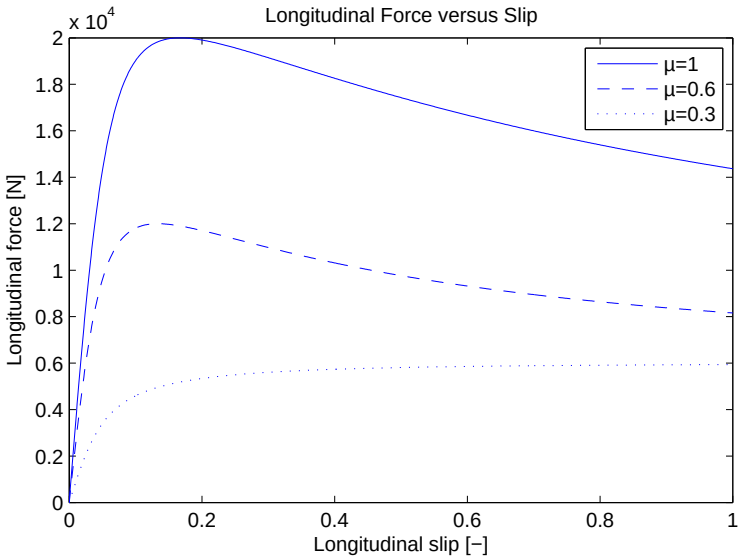

Figure 2.2 Typical shape of the longitudinal force as a function of the slip for different road conditions. The load is set to 20 000 N. The curves are generated by the Pacejka formula.

HSRI Tire Model

Another formula often used to model lateral forces is the *Highway Safety Research Institute (HSRI) Tire Model*[1]. The following equation is taken from [Klěcka, 2007]:

$$F_y = \begin{cases} C_\alpha \cdot \frac{\tan\alpha}{1+\lambda} & \text{if } s_r \leq 0.5 \\ C_\alpha \cdot \frac{\tan\alpha}{1+\lambda} \cdot \frac{s_r - 0.25}{s_r^2} & \text{if } s_r > 0.5 \end{cases}$$

where

$$s_r = \frac{\sqrt{(C_\lambda \lambda)^2 + (C_\alpha \tan\alpha)^2}}{\mu(1+\lambda)F_z}$$

and C_α and C_λ denote the initial slopes of the lateral and the longitudinal force curves, respectively. This model generates a smoothly saturating curve which can be seen in Figure 2.3, and has the advantage that it models combined longitudinal and lateral slip.

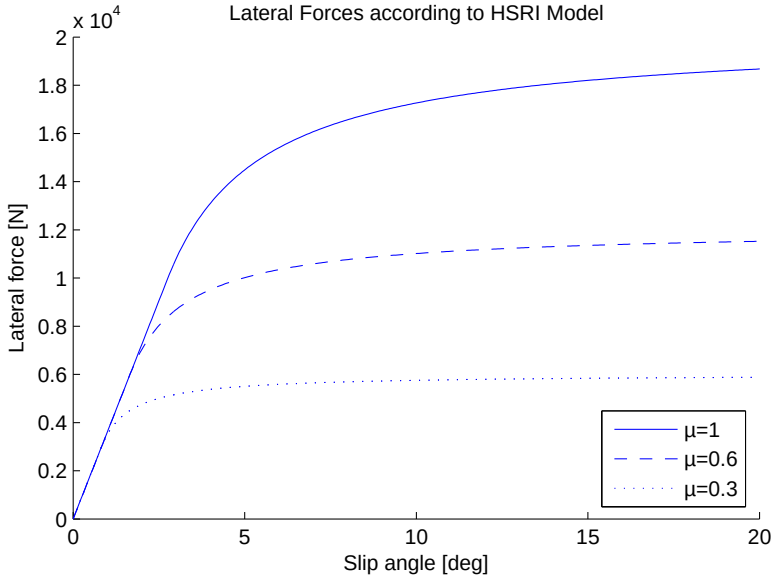

Figure 2.3 Lateral force as a function of wheel slip angle generated by the HSRI model for various friction coefficients. The load is 20 000 N.

Linear Model

As seen from Figure 2.2, for low slip values the forces can be approximated to be linear. Then a suitable model for the forces may be

$$F_x \approx C_\lambda \lambda \tag{2.5}$$

$$F_y \approx C_\alpha \alpha \tag{2.6}$$

The constants, denoted cornering and longitudinal stiffness, can be estimated from experiments.

[1] Also known as the Dugoff Tire Model

Combined Slip

Two of the three models discussed above does not take into account that the forces are dependent on both longitudinal and lateral slip at the same time. It is important when constructing the ESP in later chapters to be aware of the impact longitudinal slip has on the lateral forces generated by the tires and vice versa.

One way to model combined slip is to use the idea of the *friction ellipse*. The idea is that the longitudinal and lateral forces are bounded by their maximum values $F_{x,max}$ and $F_{y,max}$, yielding

$$\left(\frac{F_x}{F_{x,max}}\right)^2 + \left(\frac{F_y}{F_{y,max}}\right)^2 = 1.$$

When using the brakes as actuators the longitudinal forces can be seen as control inputs, and then the above equation can be used to calculate F_y. $F_{y,max}$ can be taken from a suitable tire model, for example the Pacejka formula or the HSRI model, and $F_{x,max}$ can be taken as the product of μ and F_z.

By assuming that both the longitudinal and the lateral force saturate, and are hence given by $F_{x,max} = F_{y,max} = \mu F_z$, the ellipse transforms into a circle, the so called *Kamm-circle*. This assumption, together with the approximation $\sin(\alpha) \approx \alpha$, yields the following formula [Isermann, 2006]:

$$F_x = \frac{\lambda}{\sqrt{\lambda^2 + \alpha^2}} \cdot \mu F_z \tag{2.7}$$

$$F_y = \frac{\alpha}{\sqrt{\lambda^2 + \alpha^2}} \cdot \mu F_z \tag{2.8}$$

Figure 2.4 shows how the lateral force changes with λ for some given values of α according to (2.8). The above equations, (2.7) and (2.8), accurately capture the effects of combined slip when the forces saturate. Of course, the impact of α on the longitudinal force can also be illustrated by Figure 2.4.

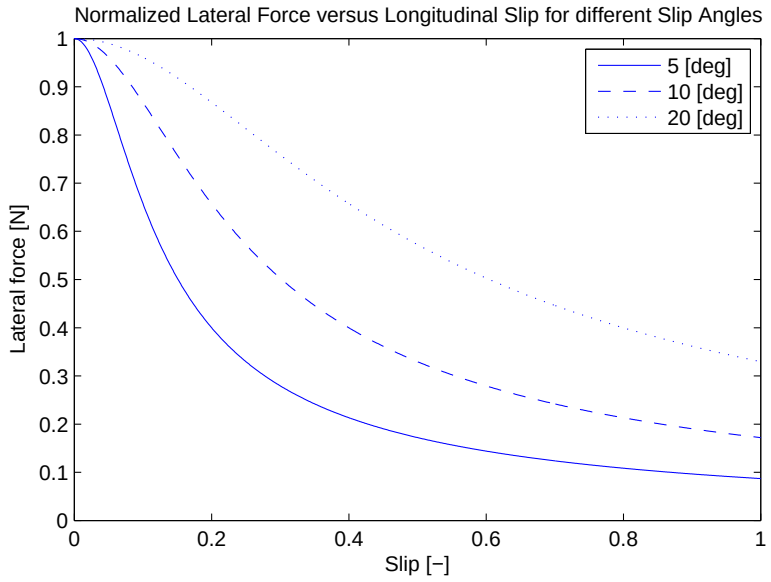

Figure 2.4 Longitudinal slip impact on the lateral force for some values of α taken from (2.8).

2.3 Wheel Modeling

In this section a model of the wheels will be derived to be able to develop control systems for the ABS and the ASR. The actuators used for the ABS are for obvious reasons the brakes. For the ASR there are several possible control outputs, including using the brakes and/or reducing engine torque. In this thesis the brakes are mostly used since then it is possible to intervene on the spinning wheel only. The ASR will also have the possibility to increase/reduce engine torque, but only when absolutely necessary. A further advantage of using the brakes is the faster dynamics of the brakes compared to the engine.

The wheels are modeled as rotating masses with driving and braking torques and road contact tire forces. When initiating the brake or drive pedal a torque is induced over the wheels, here referred to as M_B and M_A, which makes the wheels decelerate or accelerate. In the case of braking the torque comes from an increase in brake pressure P_B, whereas it in the case of accelerating comes from an increase in engine power.

Braking

In the case of braking, the situation for the wheels is as shown in Figure 2.5.

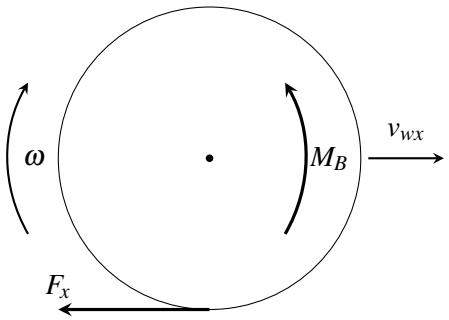

Figure 2.5 Wheel model in case of braking

From a torque balance[2] about the center of the wheel and a force balance in the longitudinal direction, one can conclude that

$$I_w\dot{\omega} = -M_B + rF_x \tag{2.9}$$

$$m^*\dot{v}_{wx} = -F_x \tag{2.10}$$

The notation is as follows:

- I_w is the moment of inertia of the wheel
- m^* is the mass resting on the wheel
- ω is the angular velocity of the wheel
- v_{wx} is the longitudinal velocity at the wheel
- r is the effective radius of the wheel
- F_x is the longitudinal force acting on the wheel which, as said before, is a nonlinear function depending on several variables

[2]The derivation of the left hand side of (2.9) in a general case is found at page 18.

To be able to build up a differential equation for the ABS (2.1) is differentiated with respect to the two variables v_{wx} and ω, which yields

$$\dot{\lambda} = -\frac{\partial\left(1-\frac{r\omega}{v_{wx}}\right)}{\partial v_{wx}} + \frac{\partial\left(1-\frac{r\omega}{v_{wx}}\right)}{\partial \omega} = \frac{r\omega}{v_{wx}^2}\dot{v}_{wx} - \frac{r}{v_{wx}}\dot{\omega}. \tag{2.11}$$

Insertion of (2.9) and (2.10) leads to

$$\dot{\lambda} = -\left(\frac{r\omega}{v_{wx}^2} + \frac{r^2 m^*}{v_{wx} I_w}\right)\frac{F_x}{m^*} + \frac{rM_B}{v_{wx} I_w}. \tag{2.12}$$

The brake pressure is proportional to the brake torque according to $M_B = C_B p_B$, see for example [Isermann, 2006], and from (2.1) there is the relation $1-\lambda = \frac{r\omega}{v_{wx}}$. Inserting these two equations into (2.12) produces the desired relationship between slip and brake pressure as

$$\dot{\lambda} = -\left(\frac{1-\lambda}{m^* v_{wx}} + \frac{r^2}{v_{wx} I_w}\right)F_x + \frac{rC_B P_B}{v_{wx} I_w}. \tag{2.13}$$

This is a nonlinear problem due to the nonlinear longitudinal force F_x, as mentioned above. The typical shape of F_x as a function of λ for different surfaces is shown in Figure 2.2.

Accelerating

When the driver is putting gas on the pedal the situation is instead as shown in Figure 2.6. The equations of motion are now

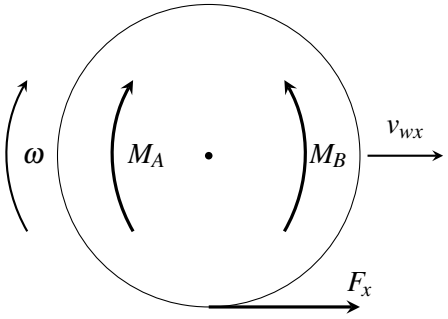

Figure 2.6 Wheel model when the driver accelerates.

$$I_w\dot{\omega} = M_A - M_B - rF_x \tag{2.14}$$

$$m^*\dot{v}_{wx} = F_x \tag{2.15}$$

The notation used here is the same as in the case of braking.

By taking the derivative of (2.2) one reaches the equation

$$\dot{\lambda} = \frac{\dot{v}_{wx}}{r\omega} - \frac{v_{wx}}{r\omega^2}\dot{\omega}. \tag{2.16}$$

To produce a relationship between λ and M_A, (2.2) is rearranged and inserted into (2.16) together with (2.14) and (2.15), yielding

$$\dot{\lambda} = \left(\frac{1+\lambda}{m^* v_{wx}} + \frac{v_{wx}}{I_w\omega^2}\right)F_x + \frac{v_{wx}}{I_w\omega^2}(M_B - M_A). \tag{2.17}$$

2.4 Load Distribution

For later use this section will model the load each wheel carries, which can vary a lot depending on the driving conditions. The load can be divided into two parts. The part of the load that is dependent on the geometry of the bus is denoted *static load distribution*. The other part, the *load transfer*, is dependent on the bus roll and pitch moments due to the height of the center of mass being different from zero. The bus is said to be rolling when it is spinning around its longitudinal axis and it is said to be pitching when spinning around its ateral axis.

The load distribution will be modeled using force and moment balances. This is a fairly simple way to perform the modeling, but as shown in [Kiencke and Nielsen, 2005] where the same approach is taken for a regular car, it still gives accurate results.

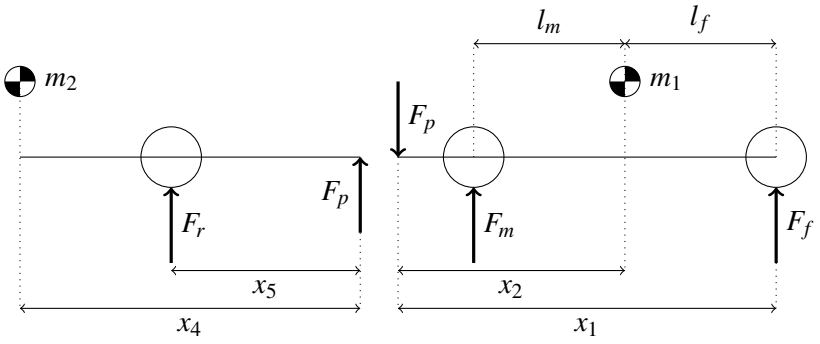

Figure 2.7 Static load distribution model with the front part to the right in the figure. The contact points are separated for easier reading.

Static Load Distribution

The center of gravity is assumed to be in the middle of the y-direction of the bus, which motivates that the normal forces on the same axle are merged and denoted F_f, F_m and F_r where the different indices stand for front, middle and rear axle, respectively. The normal force of the contact point between the two parts is denoted F_p. See Figure 2.7 for further notations.

A normal force balance for the rear part gives

$$F_r + F_p = m_2 g$$

and a torque balance around the contact point leads to the equation

$$F_r x_5 = m_2 g x_4.$$

The normal forces F_r and F_p may now be resolved as

$$\begin{aligned} F_r &= m_2 g x_4 / x_5 \\ F_p &= m_2 g (1 - x_4 / x_5) \end{aligned}$$

In the same way the tractor normal force balance

$$F_f + F_m = F_p + m_1 g$$

and the moment balance around the first axle

$$F_m(l_f + l_m) - F_p x_1 = m_1 g l_f$$

gives the normal forces on the first part as

$$F_m = \frac{m_1 g l_f + F_p x_1}{l_f + l_m}$$
$$F_f = m_1 \left(1 - \frac{l_f}{l_f + l_m}\right) + F_p \left(1 - \frac{x_1}{l_f + l_m}\right)$$

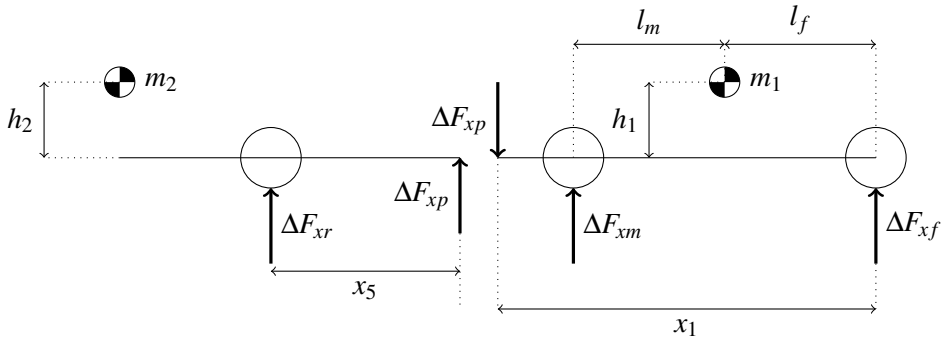

Figure 2.8 Longitudinal load transfer model.

Longitudinal Load Transfer

Wheels on the same axle are treated as one wheel, something which is motivated by the position of the center of gravity. The longitudinal load transfers are denoted with ΔF_{xf}, ΔF_{xm} and ΔF_{xr} for the front, middle and rear axle, respectively. The longitudinal acceleration for the front part is denoted a_{x1}, and for the rear part it is denoted a_{x2}. Figure 2.8 gives the other notations.

A force balance for the trailer gives

$$2\Delta F_{xr} + \Delta F_{xp} = 0,$$

and balance of moments around the link point yields

$$2\Delta F_{xr} x_5 + m_2 a_{x2} h_2 = 0.$$

Solving for the unknown variables leads to

$$\Delta F_{xr} = -\frac{m_2 a_{x2} h_2}{2x_5}, \tag{2.18}$$

and the load transfer at the link point is

$$\Delta F_{xp} = \frac{m_2 a_{x2} h_2}{x_5}.$$

The tractor forces are solved for in the same manner with the force balance

$$2\Delta F_{xf} + 2\Delta F_{xm} = \Delta F_{xp}$$

and the balance of moments around the front axle

$$2\Delta F_{xm}(l_m + l_f) + m_1 a_{x1} h_1 - \Delta F_{xp} x_1 = 0.$$

The resulting load transfer on each wheel at the first axle is then

$$\Delta F_{xf} = \frac{\Delta F_{xp}}{2}\left(1 - \frac{x_1}{l_f + l_m}\right) + \frac{m_1 h_1 a_{x1}}{2(l_f + l_m)}. \tag{2.19}$$

Likewise, for the second axle one gets

$$\Delta F_{xm} = \frac{\Delta F_{xp} x_1 - m_1 h_1 a_{x1}}{2(l_f + l_m)}. \tag{2.20}$$

Lateral Load Transfer

For the purpose of this thesis it is only of interest to model the lateral load transfer of the first part of the bus. The reason for why this is the case will be made clear in Chapter 5. The modeling is performed by assuming that the load transfer resulting from the lateral acceleration of the tractor mass is mostly carried by the tractor front axle, while the rest is carried by the tractor rear axle. The cause for this assumption is the position of the tractor center of mass. The load transfer coming from the trailer is assumed to be neglectable, motivated by the center of mass of the trailer.

The load transfer is denoted ΔF_{yf} and ΔF_{ym} for the front and rear axle of the tractor, respectively, and the lateral acceleration of the tractor is denoted a_{y1}. Let y_f and y_m be half the distance between the wheels on the both axles. A torque balance around the right wheel of the front axle leads to the equation

$$\Delta F_{yf} 2y_f = k m_1 a_{y1}.$$

This gives the load transfer at the front axle as

$$\Delta F_{yf} = k\frac{m_1 a_{y1}}{2y_f}.$$

In the same way the load transfer at the rear axle of the tractor is given by

$$\Delta F_{ym} = (1-k)\frac{m_1 a_{y1}}{2y_m}.$$

Here, k is a factor that decides how much of the load transfer is carried by each axle. In this thesis, $k = 0.6$ was found to be suitable.

2.5 Chassis Models

In this section some models are derived that may be used in different contexts in the thesis. Since the ESP is concerned with stabilizing lateral motion, the models will assume that the bus moves in the longitudinal and lateral directions only. Furthermore, the velocity is considered constant, or at least slowly time varying, in the longitudinal direction. The coordinate systems used are the vehicle-fixed and the earth-fixed. The vehicle-fixed coordinate system, denoted 'V', is moving. Therefore it is needed to express it in the inertial earth-fixed system, 'E', when dealing with equations of motion.

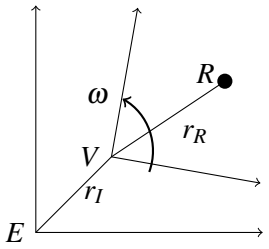

Figure 2.9 A picture showing the inertial coordinate system, E, and the non-inertial system, here denoted V.

Consider a point R described by the vector r_R relative to V, and assume that V is rotating with angular velocity ω relative to the inertial frame E. The expression for the time derivative of the vector r_R in the inertial frame is then

$$\left(\frac{dr_R}{dt}\right)_E = \left(\frac{dr_R}{dt}\right)_V + \omega \times r_R, \tag{2.21}$$

and because planar motion is assumed the expression for the angular velocity is

$$\omega = \begin{pmatrix} 0 \\ 0 \\ \dot{\psi} \end{pmatrix}.$$

If it is assumed that the moving coordinate system (the vehicle) is translated by a vector r_I from E with velocity $d(r_I)/dt = v$ relative to the inertial frame, then the velocity with respect to E of R described by the vector r_R relative to V is, by using (2.21),

$$\left(\frac{dr_R}{dt}\right)_E = v_R = v + \left(\frac{dr_R}{dt}\right)_V + \omega \times r_R. \tag{2.22}$$

For clarity, Figure 2.9 shows the situation. In the following derivations, (2.21) and (2.22) will be used.

Linear Linked-Bus Model

The model derived in this section will be linear, and the derivations will be based on those found in [Gäfvert *et al.*, 2000], although the model derived there is for a truck-trailer combination. Let the coordinate system for the front part of the bus be denoted '1', and let '2' denote the rear part system. To express a vector in frame 2 in the coordinates of frame 1 the following transformation matrix is used:

$$\begin{pmatrix} \cos\Delta\psi & -\sin\Delta\psi & 0 \\ \sin\Delta\psi & \cos\Delta\psi & 0 \\ 0 & 0 & 1 \end{pmatrix}. \tag{2.23}$$

The connection between the two parts will be modeled as a single point, p, with forces acting on it. For easier elimination of the contact forces the origins of the two vehicle-fixed coordinate systems will be placed at the contact point. The longitudinal velocity will be assumed constant or slowly changing, and therefore the dynamics in the longitudinal direction is neglected. The equations of motion are first stated for an arbitrary point. These are extended to a rigid vehicle, and later on the equations for the articulated vehicle are derived.

Equations of Motion for a Point First consider a point R with position vector $r_R = (x \quad y)^T$ with respect to the origin of a non-inertial frame V, assumed constant in this frame. The non-inertial frame V has translational velocity $v_V = (v_x \quad v_y)^T$ with respect to the inertial system. Then the velocity of R with respect to E is, by using (2.22),

$$\left(\frac{dr_R}{dt}\right)_E = v_R = v_V + \omega \times r_R. \tag{2.24}$$

By applying (2.21) on (2.24) the acceleration in the inertial frame is given by

$$\begin{aligned}\left(\frac{d^2 r_R}{dt^2}\right)_E = \left(\frac{dv_R}{dt}\right)_E = a_R &= \left(\frac{d}{dt}\right)_V (v_V + \omega \times r_R) + \omega \times (v_V + \omega \times r_R) \\ &= \left(\frac{d\omega}{dt}\right)_V \times r_R + \left(\frac{dv_V}{dt}\right)_V + \omega \times (\omega \times r_R) + \omega \times v_V \end{aligned} \tag{2.25}$$

If the components of the different parts are inserted into (2.24) and (2.25) the equations change to

$$v_R = \begin{pmatrix} v_x - \dot{\psi} y \\ v_y + \dot{\psi} x \end{pmatrix} \tag{2.26}$$

and

$$a_R = \begin{pmatrix} -\ddot{\psi} y - \dot{\psi}^2 x - \dot{\psi} v_y \\ \dot{v}_y + \ddot{\psi} x - \dot{\psi}^2 y + \dot{\psi} v_x \end{pmatrix}. \tag{2.27}$$

Equations of Motion for a Non-Linked Vehicle Next consider a rigid vehicle, for example a car, that has mass m and CoG located at $r_{CoG} = (x_{CoG} \quad y_{CoG})^T$ compared to the origin of the vehicle frame. The force acting on the vehicle is denoted $F = (0 \quad F_y)^T$, and the moment acting on the vehicle is $M = (0 \quad 0 \quad M_z)^T$ with respect to the origin of the vehicle frame.

A force equilibrium in the lateral direction gives that

$$m\left(\frac{dv_y}{dt}\right)_E = ma_y = F_y.$$

With (2.27) inserted the equation becomes

$$m(\dot{v}_y + \ddot{\psi} x_{CoG} - \dot{\psi}^2 y_{CoG} + \dot{\psi} v_x) = F_y.$$

A torque equilibrium, Euler's second law, about the origin yields

$$\left(\frac{dH_V}{dt}\right)_E = M,$$

and the angular momentum H_V is found by integrating $r_R \times d(m_R v_R)$ over the vehicle for all points R as

$$H_V = \int r_R \times d(m_R v_R).$$

By using (2.21) and (2.22) the expression can be expanded to

$$\begin{aligned}
&\left(\frac{dH_V}{dt}\right)_E = \left(\frac{dH_V}{dt}\right)_V + \omega \times H_V = \int r_R \times dm_R \left(\frac{dv_R}{dt}\right)_V \\
&= \int r_R \times dm_R \left(\frac{d(v_V + \omega \times r_R)}{dt}\right)_V \\
&= \int r_R \times dm_R \left[\left(\frac{d}{dt}\right)_V v_V + \left(\left(\frac{d}{dt}\right)_V \omega\right) \times r_R\right] \\
&= \int (x \quad y \quad 0)^T \times dm_R \left[(\dot{v}_x \quad \dot{v}_y \quad 0)^T + (0 \quad 0 \quad \ddot{\psi})^T \times (x \quad y \quad 0)^T\right] \\
&= \int (0 \quad 0 \quad (x^2+y^2) dm_R \ddot{\psi})^T + \int (0 \quad 0 \quad x dm_R \dot{v}_y)^T + \int (0 \quad 0 \quad -y dm_R \dot{v}_x)^T \\
&= (0 \quad 0 \quad M_z)^T
\end{aligned} \tag{2.28}$$

An integration[3] over the body results in

$$\begin{pmatrix} 0 \\ 0 \\ I_V \ddot{\psi} + m x_{CoG} \dot{v}_y - m y_{CoG} \dot{v}_x \end{pmatrix} = \begin{pmatrix} 0 \\ 0 \\ M_z \end{pmatrix}.$$

The expression

$$I_V = \int (x^2 + y^2) dm_R$$

can be found by using a known result which states that it is possible to calculate the moment of inertia with respect to a point, in this case the origin of the vehicle frame, through translation of the moment of inertia with respect to the center of gravity I_{zz} as

$$I_V = (x_{CoG}^2 + y_{CoG}^2) m + I_{zz}.$$

To summarize things, the equations of motion of interest are

$$m(\dot{v}_y + \ddot{\psi} x_{CoG} - \dot{\psi}^2 y_{CoG} + \dot{\psi} v_x) = F_y \tag{2.29}$$

$$I_V \ddot{\psi} + m x_{CoG} \dot{v}_y - m y_{CoG} \dot{v}_x = M_z \tag{2.30}$$

Equations of Motion for an Articulated Vehicle The bus is shown in Figure 2.10. Denote the sum of the lateral forces of the tractor coming from the tires for ΣF_{y1}. Likewise, ΣF_{y2} is used for the sum of the trailer's lateral forces. The total moment coming from the tires is denoted ΣM_{z1} and ΣM_{z2}. If δ is assumed to be small, it is seen from Figure 2.10 that these quantities are given by

$$\begin{aligned}
\Sigma F_{y1} &= F_{y1} + F_{y2} + F_{y3} + F_{y4} \\
\Sigma F_{y2} &= F_{y5} + F_{y6} \\
\Sigma M_{z1} &= x_1(F_{y1} + F_{y2}) + x_3(F_{y3} + F_{y4}) + y_f(F_{x1} - F_{x2}) + y_m(F_{x3} + F_{x4}) \\
\Sigma M_{z2} &= -x_5(F_{y5} + F_{y6}) + y_r(F_{x5} - F_{x6})
\end{aligned}$$

From (2.29) and (2.30) the equations of motion of the articulated bus become

[3] The integration should be interpreted as integration over each component

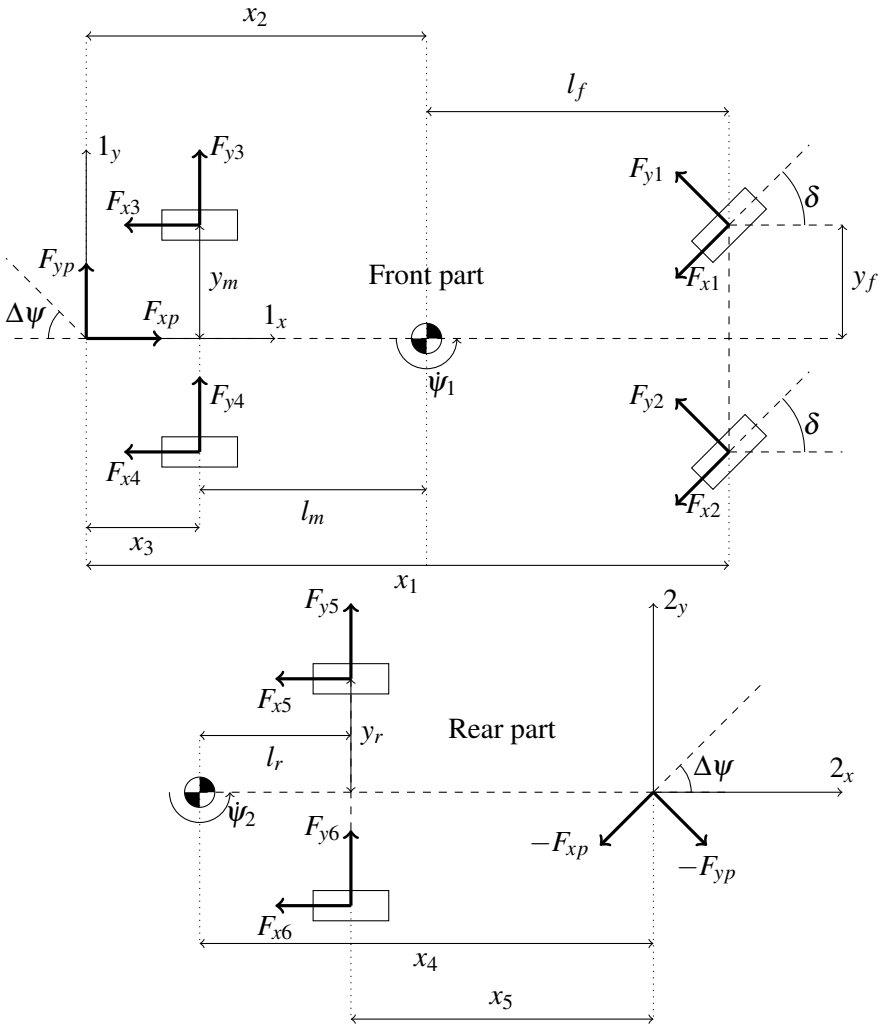

Figure 2.10 A planar model of the linked bus with forces acting on it. The vehicle-fixed coordinate systems are also shown and they both have the contact point as origin. The z-component of the coordinate systems are directed outwards in the figure. Note the definition of the longitudinal forces. Also note that the steering angle is assumed to be equal on each wheel, something which is not entirely true in reality. There are four wheels on the middle and rear axle in reality, but they are for simplicity lumped together. The sketch of the rear part is transformed by $\Delta\psi$ degrees compared to its real placement.

$$
\begin{aligned}
m_1(\dot{v}_{y1} + \ddot{\psi}_1 x_2 + \dot{\psi}_1 v_{x1}) &= \Sigma F_{y1} + F_{yp} \\
I_1 \ddot{\psi}_1 + m_1 x_2 \dot{v}_{y1} &= \Sigma M_{z1} \\
m_2(\dot{v}_{y2} - \ddot{\psi}_2 x_4 + \dot{\psi}_2 v_{x2}) &= \Sigma F_{y2} - F_{xp}\sin\Delta\psi - F_{yp}\cos\Delta\psi \\
I_2 \ddot{\psi}_2 - m_2 x_4 \dot{v}_{y2} &= \Sigma M_{z2}
\end{aligned}
$$

A small articulation angle is assumed, thus motivating the approximations $\cos\Delta\psi \approx 1$ and $\sin\Delta\psi \approx \Delta\psi$. Then the equations of motion for the articulated bus translate to

$$
\begin{aligned}
m_1(\dot{v}_{y1} + \ddot{\psi}_1 x_2 + \dot{\psi}_1 v_{x1}) &= \Sigma F_{y1} + F_{yp} \\
I_1 \ddot{\psi}_1 + m_1 x_2 \dot{v}_{y1} &= \Sigma M_{z1} \\
m_2(\dot{v}_{y2} - \ddot{\psi}_2 x_4 + \dot{\psi}_2 v_{x2}) &= \Sigma F_{y2} - F_{yp} - F_{xp}\Delta\psi \\
I_2 \ddot{\psi}_2 - m_2 x_4 \dot{v}_{y2} &= \Sigma M_{z2}
\end{aligned}
$$

The term $F_{xp}\Delta\psi$ is neglected because the forward velocity is assumed constant. The contact force F_{yp} can be eliminated as

$$m_1(\dot{v}_{y1} + \ddot{\psi}_1 x_2 + \dot{\psi}_1 v_{x1}) + m_2(\dot{v}_{y2} - \ddot{\psi}_2 x_4 + \dot{\psi}_2 v_{x2}) = \Sigma F_{y1} + \Sigma F_{y2} \tag{2.31}$$

$$I_1\ddot{\psi}_1 + m_1 x_2 \dot{v}_{y1} = \Sigma M_{z1} \tag{2.32}$$

$$I_2\ddot{\psi}_2 - m_2 x_4 \dot{v}_{y2} = \Sigma M_{z2} \tag{2.33}$$

The small articulation angle assumption gives that $v_{x1} \approx v_{x2}$ and $v_{y1} \approx v_{y2}$. Furthermore, if the velocity of the origins of the reference systems is v the acceleration at the contact point can from (2.21) be expressed as

$$\left(\frac{dv}{dt}\right)_1 + \omega_1 \times v = \left(\frac{dv}{dt}\right)_2 + \omega_2 \times v, \tag{2.34}$$

which is the same as

$$\left(\frac{dv_1}{dt}\right)_1 (\omega_1 - \omega_2) \times v_1 = \left(\frac{dv_2}{dt}\right)_2 \tag{2.35}$$

in frame 1 and 2, respectively, since the two coordinate systems have the same basis vector in the z-direction. In vector notation (2.35) is expressed as

$$\begin{pmatrix} \dot{v}_{x1} + (\dot{\psi}_1 - \dot{\psi}_2)v_{y1} \\ \dot{v}_{y1} - (\dot{\psi}_1 - \dot{\psi}_2)v_{x1} \\ 0 \end{pmatrix}_1 = \begin{pmatrix} \dot{v}_{x2} \\ \dot{v}_{y2} \\ 0 \end{pmatrix}_2 .$$

The expression on the right hand side can be translated to system 1 by using (2.23) but, since $\Delta\psi$ is assumed to be small, the transformation matrix is approximately equal to the unity matrix, and the result is that the acceleration of the trailer in the y-direction is

$$\dot{v}_{y2} = \dot{v}_{y1} - (\dot{\psi}_1 - \dot{\psi}_2)v_{x1}. \tag{2.36}$$

With (2.36) and the approximations of the velocity of the trailer inserted into (2.31)-(2.33), the following equations of motion are generated:

$$\begin{aligned} (m_1 + m_2)(\dot{v}_{y1} + \dot{\psi}_1 v_{x1}) + m_1\ddot{\psi}_1 x_2 - m_2\ddot{\psi}_2 x_4 &= \Sigma F_{y1} + \Sigma F_{y2} \\ I_1\ddot{\psi}_1 + m_1 x_2 \dot{v}_{y1} &= \Sigma M_{z1} \\ I_2\ddot{\psi}_2 - m_2 x_4(\dot{v}_{y1} + (\dot{\psi}_1 - \dot{\psi}_2)v_{x1}) &= \Sigma M_{z2} \end{aligned}$$

From Figure 2.10 one can note that $\Delta\psi = \psi_1 - \psi_2$, which changes the equations of motion to

$$(m_1 + m_2)(\dot{v}_{y1} + \dot{\psi}_1 v_{x1}) + m_1\ddot{\psi}_1 x_2 - m_2\ddot{\psi}_2 x_4 = \Sigma F_{y1} + \Sigma F_{y2} \tag{2.37}$$

$$I_1\ddot{\psi}_1 + m_1 x_2 \dot{v}_{y1} = \Sigma M_{z1} \tag{2.38}$$

$$I_2\ddot{\psi}_2 - m_2 x_4(\dot{v}_{y1} + v_{x,1}\dot{\psi}_1 - \dot{\psi}_2 v_{x1}) = \Sigma M_{z2} \tag{2.39}$$

The attention is now turned to the right hand side part of the equations of motion. A number of assumptions will be used to simplify the equations:

1. First, the steering angle δ is assumed small.

2. The second assumption is that the slip angles of the two wheels on the same axle are equal. This assumption makes it possible to express the lateral forces at each axle as arising from a wheel centered in the middle of the axle.
3. The third assumption is that the slip angles of the wheels are small, which enables the use the linear force approximation in Section 2.2.

The longitudinal forces are not lumped together since this would restrict the usefulness of the model for control purpose. With the approximations inserted the right hand side of the equations of motion are

$$\begin{aligned}
\Sigma F_{y1} &= C_{\alpha_f}\alpha_f + C_{\alpha_m}\alpha_m \\
\Sigma F_{y2} &= C_{\alpha_r}\alpha_r \\
\Sigma M_{z1} &= x_1 C_{\alpha_f}\alpha_f + x_3 C_{\alpha_m}\alpha_m + y_f(F_{x1} - F_{x2}) + y_m(F_{x3} - F_{x4}) \\
\Sigma M_{z2} &= -x_5 C_{\alpha_r}\alpha_r + y_r(F_{x5} - F_{x6})
\end{aligned}$$

By forming velocity balance equations in both directions about every wheel and dividing the two equations, see Figure 2.11, the slip angles can be expressed as

$$\tan(\delta - \alpha_f) = \frac{l_f\dot{\psi}_1 + ||v_1||\sin\beta_1}{||v_1||\cos\beta_1}$$

for the front wheel. Similarly, for the second wheel

$$\tan(\alpha_m) = \frac{l_m\dot{\psi}_1 - ||v_1||\sin\beta_1}{||v_1||\cos\beta_1}.$$

Finally, for the third wheel

$$\tan(\alpha_r) = \frac{-l_r\dot{\psi}_2 - ||v_2||\sin\beta_2}{||v_2||\cos\beta_2}.$$

At stable driving conditions the lateral velocity is small compared to the longitudinal. This implies that $v_i \approx v_{xi}$, $\sin\beta_i \approx \beta_i \approx \frac{v_{yi}}{v_{xi}}$ and $\cos\beta_i \approx 1$. The final expressions for the slip angles are given if one puts $\tan\alpha = \alpha$. This can be done since the wheels' slip angles are assumed to be small.

$$\alpha_f = \delta - \frac{1}{v_{x1}}(v_{y1} + l_f\dot{\psi}_1) \tag{2.40}$$

$$\alpha_m = -\frac{1}{v_{x1}}(v_{y1} - l_m\dot{\psi}_1) \tag{2.41}$$

$$\alpha_r = -\frac{1}{v_{x1}}(v_{y1} + l_r\dot{\psi}_2) \tag{2.42}$$

The final expression for the linear equations of motion are now found by using the approximations (2.40)-(2.42) in the right hand side of (2.37)-(2.39) and introducing the state vector $\chi = (v_{y1} \quad \dot{\psi}_1 \quad \dot{\psi}_2)^T$:

$$H\dot{\chi} = A\chi + Bu, \tag{2.43}$$

where

$$H = \begin{pmatrix} m_1 + m_2 & m_1x_2 & -m_2x_4 \\ m_1x_2 & I_1 & 0 \\ -m_2x_4 & 0 & I_2 \end{pmatrix}.$$

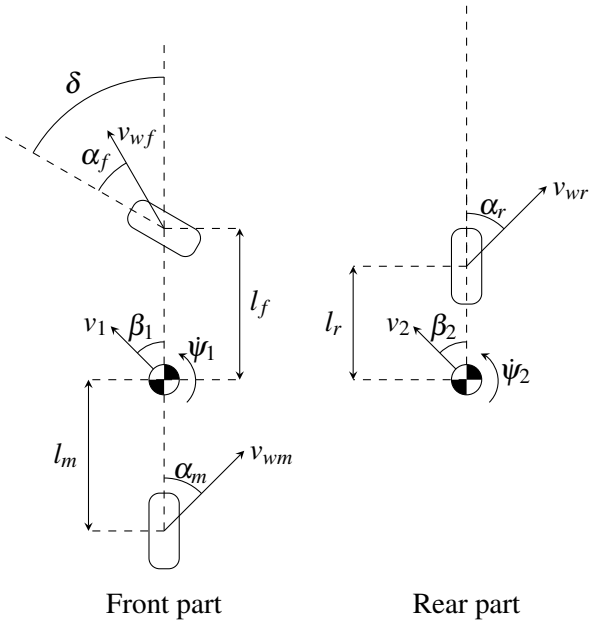

Figure 2.11 A simplified sketch of the one-track model for both parts of the bus. From this figure expressions for α_i can be found by forming velocity balances in both directions around the wheels.

The element on row $i = 1 \ldots 3$ and column $j = 1 \ldots 3$, a_{ij}, of A is

$$
\begin{aligned}
a_{11} &= -\frac{1}{v_{x1}} \left(C_{\alpha_f} + C_{\alpha_m} + C_{\alpha_r} \right) \\
a_{12} &= -\frac{1}{v_{x1}} \left(l_f C_{\alpha_f} - l_m C_{\alpha_m} \right) - (m_1 + m_2) v_{x1} \\
a_{13} &= -\frac{l_r C_{\alpha_r}}{v_{x1}} \\
a_{21} &= -\frac{1}{v_{x1}} \left(x_1 C_{\alpha_f} + x_3 C_{\alpha_m} \right) \\
a_{22} &= -\frac{1}{v_{x1}} \left(x_1 l_f C_{\alpha_f} - x_3 l_m C_{\alpha_m} \right) \\
a_{23} &= 0 \\
a_{31} &= \frac{x_5 C_{\alpha_r}}{v_{x1}} \\
a_{32} &= m_2 x_4 v_{x1} \\
a_{33} &= \frac{x_5 l_r C_{\alpha_r}}{v_{x1}} - m_2 x_4 v_{x1}
\end{aligned}
$$

The matrix B is

$$
B = \begin{pmatrix}
C_{\alpha_f} & 0 & 0 & 0 & 0 & 0 & 0 \\
x_1 C_{\alpha_f} & y_f & -y_f & y_m & -y_m & 0 & 0 \\
0 & 0 & 0 & 0 & 0 & y_r & -y_r
\end{pmatrix},
$$

and the input vector u is given by

$$u = \begin{pmatrix} \delta \\ F_{x1} \\ F_{x2} \\ F_{x3} \\ F_{x4} \\ F_{x5} \\ F_{x6} \end{pmatrix}.$$

This linear model has the steering angle at the front wheels δ and the longitudinal forces as inputs, and is therefore suited for control applications.

Linear One-Track Model

In this section a model of the dynamics of the front part of the rigid bus will be derived. The origin of the vehicle-fixed coordinate system will in this case be at the center of gravity. This makes the equations less complex. For example, in the equations for the derivation above all parts containing r_{CoG} would become zero.

A force equilibrium in the y-direction and a torque equilibrium around the z-axis of the tractor yields

$$\begin{aligned} m_1 a_{y1} &= F_{y1}\cos\delta - F_{x1}\sin\delta + F_{y2}\cos\delta - F_{x2}\sin\delta \\ &\quad + F_{y3} + F_{y4} + F_{yp} \end{aligned} \tag{2.44}$$

$$\begin{aligned} I_{zz1}\ddot{\psi}_1 &= F_{y1}(l_f\cos\delta + y_f\sin\delta) + F_{x1}(y_f\cos\delta - l_f\sin\delta) \\ &\quad + F_{y2}(l_f\cos\delta - y_f\sin\delta) - F_{x2}(y_f\cos\delta + l_f\sin\delta) \\ &\quad - l_m F_{y3} + y_m F_{x3} - (l_m F_{y4} + y_m F_{x4}) - x_2 F_{yp} \end{aligned} \tag{2.45}$$

By lumping together the wheels on the same axle inte one single wheel and neglecting the longitudinal forces, together with the assumption of small steering inputs, the above equations are simplified to

$$\begin{aligned} m_1 a_{y1} &= F_{yf} + F_{ym} + F_{yp} \\ I_{zz1}\ddot{\psi}_1 &= l_f F_{yf} - l_m F_{ym} - x_2 F_{yp} \end{aligned}$$

for the tractor. To further simplify matters it is, just as for the previously derived model, assumed that the wheels' slip angles are small. The articulation angle is also assumed to be small, and therefore the lateral force F_{yp} is neglected. With these approximations inserted the equations are changed to

$$\begin{aligned} m_1 a_{y1} &= C_{\alpha_f}\alpha_f + C_{\alpha_m}\alpha_m \\ I_{zz1}\ddot{\psi}_1 &= l_f C_{\alpha_f}\alpha_f - l_m C_{\alpha_m}\alpha_m \end{aligned}$$

The next step is to use relation (2.21) to express the lateral acceleration in its components. The lateral acceleration at the center of mass of the tractor can be divided into two parts, according to (2.25), which are

$$a_1 = \dot{v}_1 + \omega \times v_1 = \begin{pmatrix} 0 \\ \dot{v}_{y1} \\ 0 \end{pmatrix} + \begin{pmatrix} 0 \\ 0 \\ \dot{\psi}_1 \end{pmatrix} \times \begin{pmatrix} v_{x1} \\ v_{y1} \\ 0 \end{pmatrix} = \begin{pmatrix} -v_{y1}\dot{\psi}_1 \\ \dot{v}_{y1} + v_{x1}\dot{\psi}_1 \\ 0 \end{pmatrix}$$

By inserting the simplified expressions for the slip angles, (2.40)-(2.41), the expression for a_{y1} and writing the equations on state-space form the equations for the tractor are

$$\begin{pmatrix} \dot{v}_{y1} \\ \ddot{\psi}_1 \end{pmatrix} = \begin{pmatrix} -\frac{C_{\alpha_f}+C_{\alpha_m}}{m_1 v_{x1}} & \frac{l_m C_{\alpha_m} - l_f C_{\alpha_f}}{m_1 v_{x1}} - v_{x1} \\ \frac{l_m C_{\alpha_m} - l_f C_{\alpha_f}}{I_{zz1} v_{x1}} & -\frac{l_f^2 C_{\alpha_f} + l_m^2 C_{\alpha_m}}{I_{zz1} v_{x1}} \end{pmatrix} \begin{pmatrix} v_{y1} \\ \dot{\psi}_1 \end{pmatrix} + \begin{pmatrix} \frac{C_{\alpha_f}}{m_1} \\ \frac{l_f C_{\alpha_f}}{I_{zz1}} \end{pmatrix} \delta \tag{2.46}$$

There were some assumptions made when deriving the two models which limit the situations for when they are valid:

- Only planar motion
- Small steering angle δ[4]
- Small articulation angle $\Delta\psi$
- Linear tire forces
- Approximation of α
- Constant longitudinal velocity
- $v_x \gg v_y$

The most crucial approximations for the validity of the models are the linear tire force and constant velocity approximations. These approximations can, however, be taken care of, as will be shown in Chapter 5. Experiments on dry asphalt have shown that the linear one-track model for a regular car is valid for lateral accelerations up to $0.4g$.

2.6 Summary

In this chapter different models for different purposes have been discussed. Different tire models were explained in Section 2.2. The most common tire model used in literature is the Pacejka Formula, but the HSRI Tire Model also finds its use. The linear tire model is also common due to its simplicity and accurateness in the low-slip region.

The wheel model that was derived in Section 2.3 is a rather simple model which neglects, for example, suspension dynamics and the bus' pitching motion while braking. Nevertheless, it is useful in the context of slip control design, something which will be discussed in the next chapter.

The load transfer model accurately captures the impact the acceleration has on the distribution of the load, and it will be used in Chapter 5.

When it comes to the chassis models, both models discussed in this chapter are rather simple. The first model, (2.43), is more detailed, taking into account the longitudinal forces and the dynamics of the trailer. This makes the model suitable for control design, at least during stable driving conditions. The second model assumes that no longitudinal forces are present, which together with the neglection of the trailer dynamics severely limits the use of it for control purposes. Still, the model can be expected to mimic the dynamics of the bus relatively well during steady state driving. This of course also holds for (2.43).

[4]For the largest steering angles considered in this thesis, this assumption only introduces a relative error of about 5-10 percent in the moment and force equations.

3. Slip Control Design

As seen in Section 2.3 the longitudinal force depends on the slip in a nonlinear fashion, where the force has a more or less pronounced peak for some value of the slip. The idea of the ABS and the ASR is to control the slip around different slip values using the brakes. For emergency braking the slip value would be that which produces maximum force, and for the ESP the value could be anything between 0 and 1. Since the design of the ABS and the ASR are nearly identical the design of the ABS is explained in depth, and only the differences between the two systems are pointed out last in the chapter. For extensive reading on slip control design and various control strategies, see [Solyom, 2002], [Petersen, 2003] and [Isermann, 2006].

3.1 ABS

Controller Choice

In Section 2.3 the relationship between λ and P_B was found to be

$$\dot{\lambda} = -\left(\frac{1-\lambda}{m^* v_{wx}} + \frac{r^2}{v_{wx} I_w}\right) F_x + \frac{r C_B}{v_{wx} I_w} P_B. \tag{3.1}$$

Neglecting the term $\frac{1-\lambda}{m^* v_{wx}}$ is possible, as it is much smaller than the other parts[1]. Then (3.1) transforms to

$$\dot{\lambda} = -\frac{r^2}{v_{wx} I_w} F_x + \frac{r C_B}{v_{wx} I_w} P_B. \tag{3.2}$$

There are, of course, several ways to adress this control problem. In [Petersen, 2003] gain-scheduled LQR controllers are used, while optimal gain-scheduled PI-controllers are designed in [Solyom, 2002]. In [Isermann, 2006] feedback linearization is employed. This thesis will use PID-controllers together with gain scheduling. Inspiration in the design procedure is taken from [Solyom, 2002].

Consider Figure 2.2 and let k_F denote the slope of the curve at a certain point. Let Δu be the difference between the actual value u and the point around which a linearization is performed. Then a linearization of (3.2) yields the linear differential equation

$$\Delta\dot{\lambda} = -\frac{r^2}{v_{wx} I_w} k_F \Delta\lambda + \frac{r C_B}{v_{wx} I_w} \Delta P_B, \tag{3.3}$$

which is a first order system whose stability depends on k_F. Since the system is stable to the left of the maximum and unstable to the right of the maximum of Figure 2.2, the dynamics of the system differs depending on if $\lambda > \lambda^*$ or $\lambda < \lambda^*$, where λ^* is the value of the slip where the maximum longitudinal force is attained. This leads to the choice of λ^* as scheduling variable, which is estimated from experiment. The value for which the peak occurs is dependent on the friction coefficient between the surface and tire, see Figure 2.2 for an example, and can also be considered a scheduling variable[2], but for simplicity in the control design this is omitted.

[1] For the considered bus this term only contributes with about 0.01 %

[2] If scheduling is also done with respect to the friction coefficient, the Pacejka formula can preferrably be used to estimate the peak.

Sampling and communication introduce time delays in the process. However, delays are not included in the design. It is known that unstable poles, especially in conjunction with time delays, set an upper limit of what can be achieved in terms of control performance, but this is not considered further here. Also neglected in the design is the brake dynamics.

The motivation for using a PID-controller is that the linearized system is of first order, and for pure first order systems asymptotic stability is ensured with a PID-controller. This can be seen by considering the poles of a first order system in feedback with the chosen controller, where the poles can be placed in the left-half plane. The inclusion of an integral term will also account for unmodeled dynamics. Furthermore, the use of a PID-controller ensures that no control errors are present in stationarity [Åström and Murray, 2008].

The transfer function for a PID-controller is as follows:

$$C_{ABS}(s) = K\left(1 + \frac{1}{sT_i} + sT_d\right) \tag{3.4}$$

As seen in (3.3) the gain is highly dependent on v_{wx}, where the system has higher bandwidth for lower velocity and vice versa. By incorporating the velocity in the controller this dependence can be reduced. Therefore the controller is extended to

$$C_{ABS}(s) = Kv_{wx}\left(1 + \frac{1}{sT_i} + sT_d\right) = Kv_{wx}\left(\frac{s^2T_iT_d + sT_i + 1}{sT_i}\right) \tag{3.5}$$

and the parameters used are the following:

$$Parameters = \begin{cases} K_1, T_{i1}, T_{d1} \text{ if } \lambda \leq \lambda^* \\ K_2, T_{i2}, T_{d2} \text{ if } \lambda > \lambda^* \end{cases}$$

where the velocity is incorporated into the proportional gain. The system has infinite gain when $v_{wx} \to 0$, which makes it practically impossible to control the system. The controller is therefore switched off for velocities less than $v_{wx} \approx 1$ m/s, and the driver will then again decide the brake pressure. It is of great importance to reach the desired slip fast, and a small overshoot is no problem. For this reason the initial state of the integral term is set when the ABS is activated.

Discretization

The controller is to be used in a bus as a digital control unit, and thus the control algorithm has to be discretized. More details about different types of discretization techniques are found in [Åström and Wittenmark, 1997].

Let $e_\lambda = \lambda_{ref} - \lambda$ be the control error. The controller can be written on the form $U = P + I + D$, where

$$\begin{aligned} P &= K_{1,2}e_\lambda \\ I &= \frac{K_{1,2}}{sT_{i1,2}}e_\lambda \\ D &= K_{1,2}T_{d1,2}se_\lambda \end{aligned}$$

The proportional part needs not to be discretized. The integral part is rewritten as

$$sI = \frac{K_{1,2}}{T_{1,2}}e_\lambda.$$

This corresponds to

$$\frac{dI}{dt} = \frac{K_{1,2}}{T_{1,2}} e_\lambda$$

in the time domain. By using the approximation

$$\dot{u} \approx \frac{u(t+T_s) - u(t)}{T_s},$$

where $T_s = 0.01$ denotes the sampling time, one gets the integral term as

$$I(t+T_s) = I(t) + \frac{K_{1,2}T_s}{T_{i1,2}} e_\lambda(t) \tag{3.6}$$

The derivative part has strictly increasing gain, leading to enhancement of noise, and therefore the approximation

$$sT_d \approx \frac{sT_d}{1+sT_d/N}$$

is used, where N decides the cut-off frequency. This approximation will give a good fit for low frequencies, but the gain will be limited depending on N for high frequencies. Since step changes in the reference may give rise to high amplification in the derivative part, the derivative will not act on the reference. The discretization used is

$$\dot{u} \approx \frac{u(t) - u(t-T_s)}{T_s},$$

leading to

$$D(t) = \frac{T_{d1,2}}{T_{d1,2}+NT_s} D(t-T_s) - \frac{K_{1,2}T_{d1,2}N}{T_{d1,2}+NT_s}(\lambda(t) - \lambda(t-T_s)).$$

Anti-Windup

The controller includes an integral term, and thus there is a risk of windup. Because of the actuator being saturated, the windup is avoided by stop updating the integral term when the actuator saturates [Åström and Wittenmark, 1997].

Stability Analysis

As help to find suitable parameters and prove stability of the system, a tool suited for the problem must be used. One method to prove stability for nonlinear systems is the nonlinear variant of the well known *Nyquist Criterion*, the *Circle Criterion*. To be able to state that theorem some theory is needed, which the reader is advised to [Khalil, 2000] and [Glad and Ljung, 2003] for more information on.

Consider the feedback connection in Figure 3.1 where $f(y,t)$ is a static nonlinearity, possibly time varying, locally Lipschitz in y and piecewise continous in t bounded as

$$\alpha y \leq \frac{f(y,t)}{y} \leq \beta y, \quad \forall y \in \mathbf{R},\ t \geq 0$$

where $\alpha, \beta \in \mathbf{R}$, $\alpha < \beta$ and $\beta \neq 0$. The feedback connection can also be written on the following form

$$\dot{x} = Ax + Bu \tag{3.7}$$

$$y = Cx \tag{3.8}$$

$$u = -f(y,t) \tag{3.9}$$

where $x \in \mathbf{R}^n$, $u, y \in \mathbf{R}^p$, (A,B) is controllable, (A,C) is observable and $f(y,t)$ is a nonlinearity as described above.

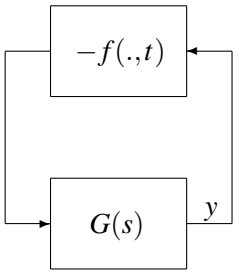

Figure 3.1 A transfer function $G(s)$ in feedback connection with a nonlinearity $f(.,t)$

DEFINITION 3.1
The origin of the system (3.7)-(3.9) is

- stable if, for each $\varepsilon > 0$, there is $\delta = \delta(\varepsilon, t_0) > 0$ such that

$$||x(t_0)|| < \delta \implies ||x(t)|| < \varepsilon, \quad \forall t \geq t_0 \geq 0. \tag{3.10}$$

- uniformly stable if, for each $\varepsilon > 0$, there is $\delta = \delta(\varepsilon) > 0$, independent of t_0, such that (3.10) is satisfied.
- unstable if it is not stable.
- asymptotically stable if it is stable and there is a positive constant $c = c(t_0)$ such that $x(t) \to 0$ as $t \to \infty$, for all $||x(t_0)|| < c$.
- uniformly asymptotically stable if it is uniformly stable and there is a positive constant c, independent of t_0, such that for all $||x(t_0)|| < c$, $x(t) \to 0$ as $t \to \infty$, uniformly in t_0; that is, for each $\nu > 0$, there is $T = T(\nu) > 0$ such that

$$||x(t)|| < \nu, \quad \forall t \geq t_0 + T(\nu), \ \forall ||x(t_0)|| < c.$$

- globally uniformly asymptotically stable if it is uniformly stable, $\delta(\varepsilon)$ can be chosen to satisfy $lim_{\varepsilon \to \infty} \delta(\varepsilon) = \infty$ and for each pair of positive numbers ν and c, there is $T = T(\nu, c) > 0$ such that

$$||x(t)|| < \nu, \quad \forall t \geq t_0 + T(\nu, c), \ \forall ||x(t_0)|| < c.$$

□

DEFINITION 3.2
The system (3.7)-(3.9) is absolutely stable if the origin is globally uniformly asymptotically stable for any nonlinearity in the given sector. It is absolutely stable with a finite domain if the origin is uniformly asymptotically stable. □

DEFINITION 3.3
$D(\alpha, \beta)$ is the closed disk in the complex plane whose diameter is the line segment connecting the points $-1/\alpha$ and $-1/\beta$. □

THEOREM 3.1—CIRCLE CRITERION
Assume that the system (3.7)-(3.9) has the transfer function $G(s)$. Then the system is absolutely stable if one of the following conditions is satisfied, as appropriate:

1. If $0 < \alpha < \beta$, the Nyquist plot of $G(s)$ does not enter the disk $D(\alpha,\beta)$ and encircles it m times in the countercklockwise direction where m is the number of poles of $G(s)$ with positive real parts.
2. If $0 = \alpha < \beta$, all poles of $G(s)$ have negative real part and the Nyguist plot of $G(s)$ lies to the right of the vertical line defined by Re[s]=$-1/\beta$.
3. If $\alpha < 0 < \beta$, all poles of $G(s)$ have negative real part and the Nyquist plot of $G(s)$ lies in the interior of the disk $D(\alpha,\beta)$.

□

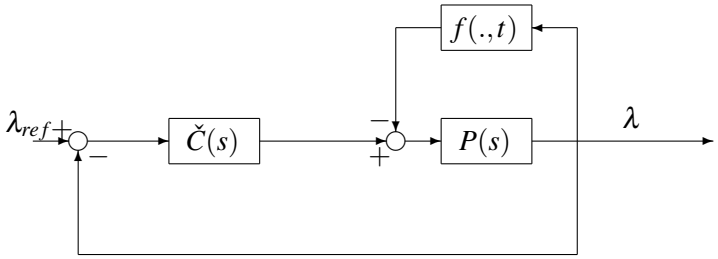

Figure 3.2 Block diagram showing nonlinearity, nominal plant and controller for the ABS.

Consider Figure 3.2 where $f(.,t) = F_x(.)r^2/I_w$, $P(s) = 1/(sv_{wx})$ and

$$\check{C}(s) = \frac{rC_BKv_{wx}}{sI_wT_i}\left(s^2T_iT_d + sT_i + 1\right),$$

where the indices of the control parameters are omitted. This is the structure of (3.2) after a Laplace transform and with the controller inserted. The goal is to find an expression which is in feedback connection with the nonlinearity $f(\lambda,t)$ the way described in Figure 3.1. Toward that end, denote the output from the nonlinearity with z and the input with λ. Setting $\lambda_{ref} = 0$ results in

$$z = f(\lambda,t) \tag{3.11}$$

and

$$\lambda = -P(s)(z + \lambda\check{C}(s)). \tag{3.12}$$

By solving (3.12) for λ and inserting (3.11) one gets

$$\lambda = -f(\lambda,t)\frac{P(s)}{1 + P(s)\check{C}(s)} = -f(\lambda,t)G(s).$$

It is seen that $G(s)$ is in feedback connection with the nonlinearity, and it is therefore possible to use Theorem 3.1 to try to conclude stability of the origin. Note that

additional dynamics can easily be incorporated into the design, for example the unmodeled brake dynamics. The bounds for the nonlinearity can be determined from experiments or worst case scenarios.

Because the ABS is concerned with slip values different from zero, it is desirable to show asymptotic stability of certain equilibrium points rather than origo itself. The fact that Theorem 3.1 assumes an equilibrium point at the origin poses no problem, since a nonzero equilibrium point can be transformed to the origin by a simple variable change, as shown next.

Let a system be

$$\begin{aligned} \dot{x} &= Ax + Bu + B_r r \\ y &= Cx \\ u &= -f(y,t) \end{aligned}$$

where r is the (constant) reference input to the system and the matrices and vectors are of appropriate dimensions. This is the system shown in Figure 3.2. Denote the corresponding equilibrium point with x_0. Also, introduce a variable change $\zeta = x - x_0$. Differentiating ζ gives as a result the equation

$$\dot{\zeta} = A\zeta - B\varphi(C\zeta),$$

where $\varphi(C\zeta) = f(C(\zeta + x_0)) - f(Cx_0)$ is a cone bounded nonlinearity which can be written as

$$\alpha \leq \frac{\varphi(y_1) - \varphi(y_2)}{y_1 - y_2} \leq \beta, \quad \forall y_1, y_2 \in \mathbf{R}. \tag{3.13}$$

Using Theorem 3.1 on this transformed system, provided that the other requirements are fulfilled, leads to the result that $\zeta = 0$ is globally uniformly asymptotically stable. Therefore the equilibrium point $x = x_0$ is globally uniformly asymptotically stable. As mentioned before, the use of a PID-controller ensures that this is the desired equilibrium point. Note that the bounds for the new nonlinearity most probably are not the same as for the original, depending on the character of $f(.,.)$.

Design Example

Let the velocity be 20 m/s. The nonlinearity is bounded as in Figure 3.3, where the nonlinearities are for friction coefficients $\mu = 1$ and $\mu = 0.7$. The resulting control parameters leads to the following Nyquist plot of $G(s)$ for the front wheels (Figure 3.4). Concluding asymptotic stability by the Circle Criterion is then possible. By changing the velocity, friction coefficient and loading conditions the conclusion that the controller is stable for all relevant combinations can be drawn. In a similar fashion the procedure can be repeated for the case when the nonlinearity is bounded to the right of the peak. Since the loading conditions and the proportional constant C_B are different for the different axles suitable control parameters will differ somewhat, but the design procedure is of course still the same.

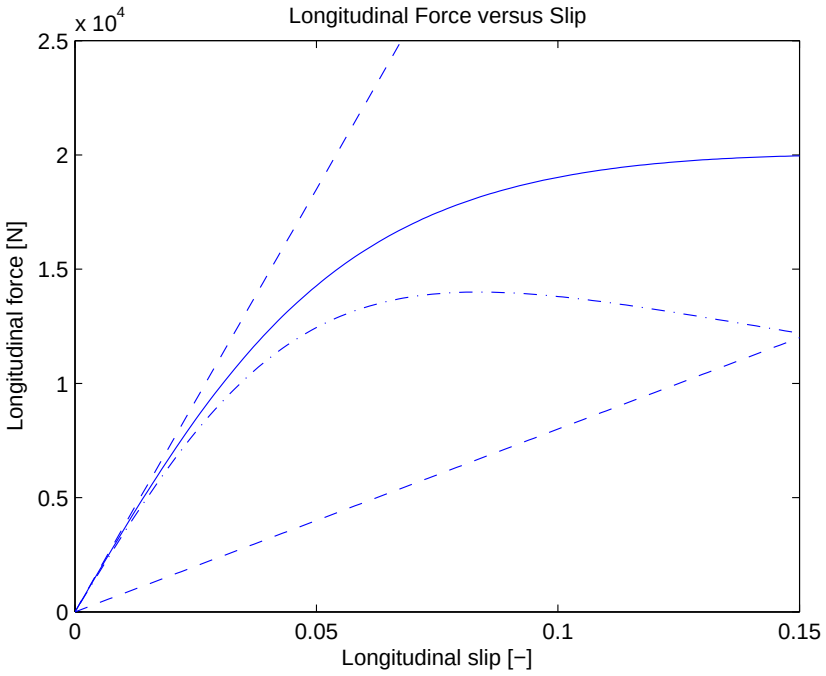

Figure 3.3 The nonlinearity $f(y,t)$ for a dry and wet road, the solid and dash-dotted lines, with a set of possible bounding slopes, shown as dashed in the plot.

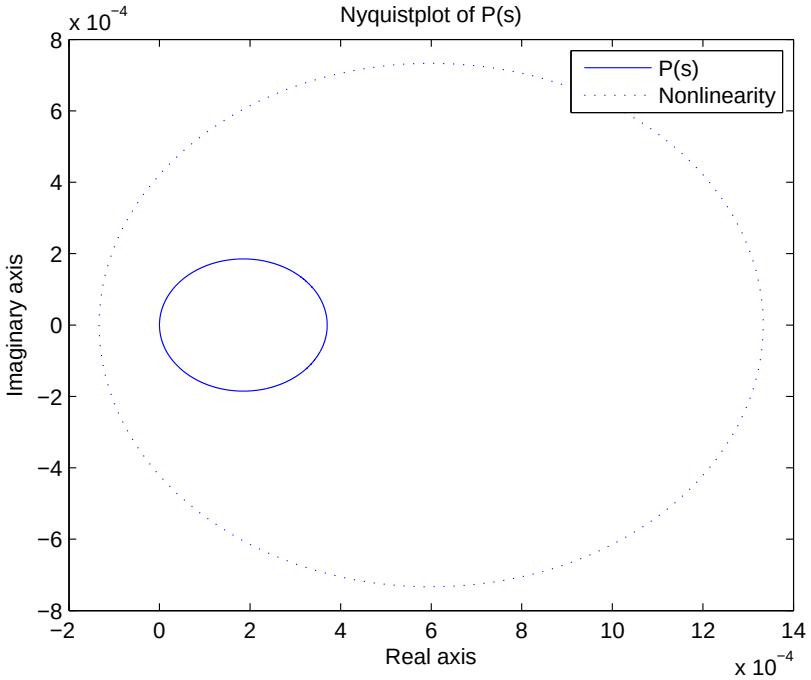

Figure 3.4 Nyquist plot of $G(s)$ for a stable set of parameters for the front wheels at a velocity of 20 m/s, and the circle defined by the nonlinearity bounds for a nonzero equilibrium point calculated as in (3.13).

3.2 ASR

As said before, the design of the ASR system is very similar to that of the ABS. The differences can be seen by comparing (2.13) and (2.17), where the later equation has dependence of v_{wx}/ω_w^2 instead of $1/v_{wx}$, and (2.17) is also dependent on the engine torque. The dependence of v_{wx}/ω_w^2 is eliminated in the same way as for the ABS. The controller also eliminates the term M_A, which is justified if this term is known. The final form of the controller for the ASR system is

$$P_B = \frac{M_A}{C_B} + \frac{\omega_w^2}{C_B v_{wx}} \left(K(\lambda_{ref} - \lambda) + \frac{K}{T_i} \int (\lambda_{ref} - \lambda) dt + K T_d \frac{d(\lambda_{ref} - \lambda)}{dt} \right),$$

which is almost identical to the ABS case. The ASR is also capable of increasing engine torque, which will be discussed more in Chapter 6. Of course, the same discretizations as for the ABS is applicable in this case as well. Since the ASR only works in the region $-0.15 \leq \lambda \leq 0$, it was sufficient to design one set of parameters only.

3.3 Summary

This chapter has been devoted to design of the ABS and the ASR. Gain-scheduled PID-controllers are used, and stability is shown with the Circle Criterion. The motivation for this was that the system is highly nonlinear, but the linearized system is of first order and can usually be controlled by PID-controllers with good result.

4. Evaluation of the Slip Control

4.1 Evaluation of the ABS

The controller should work well on everything from icy roads to dry asphalt and combinations there of, and therefore the tests carried out were the following:

1. Emergency braking on dry asphalt, roughly corresponding to $\mu = 1$.
2. Emergency braking at $\mu = 0.3$ corresponding to icy road.
3. μ-step braking, that is emergency braking on high friction ($\mu = 1$) road and thereafter low friction road ($\mu = 0.2$) a couple of metres before high friction road ($\mu = 1$) is again encountered. This corresponds to a dry road with icy spots.

In all tests the vehicle performed straight driving with a constant initial velocity. Emergency braking is started at 2 seconds during all simulations. The ABS is activated when the slip due to emergency braking enters the unstable region of the force curve, where the risk of wheel lock is high. The limit during the simulations was set to 0.15, which matches the peak at high μ.

Inf Figure 5.1, 5.3 and 5.5 the upper plot shows the actual slip together with the reference slip. The middle plot depicts the velocity together with the wheel's velocity $r\omega$, which gives a different view of the actual slip. A plot of the acceleration is shown to illustrate the difference in achieved braking force depending on the slip. The plots will show the states for the third wheel, that is the left wheel on the second axle. In Section B.1 the plots for the other wheels are given.

Braking on Dry Asphalt

It can be seen that the controller performs well in terms of following the reference, see Figure 4.1. At low velocities the performance detoriates, just as predicted in Section 3.1. The oscillations in the acceleration plot, Figure 4.2, that appear is due to the pitching motion of the bus and the relative speed of the tractor and trailer.

Braking on Icy Road

For low friction coefficients the controller is also seen to be performing well, according to the results in Figure 4.3, with a smooth following of the reference. Just as predicted, the slip oscillates around the reference for low velocities also in this case.

μ-Step Braking

The μ-step braking demands a bit more from the controller since a change in friction coefficient drastically changes the dynamics of the force curve, as pointed out in Figure 2.2. It can be seen in Figure 4.5 that the slip exhibits spikes when the surface changes, although the controller quickly restrains the effects.

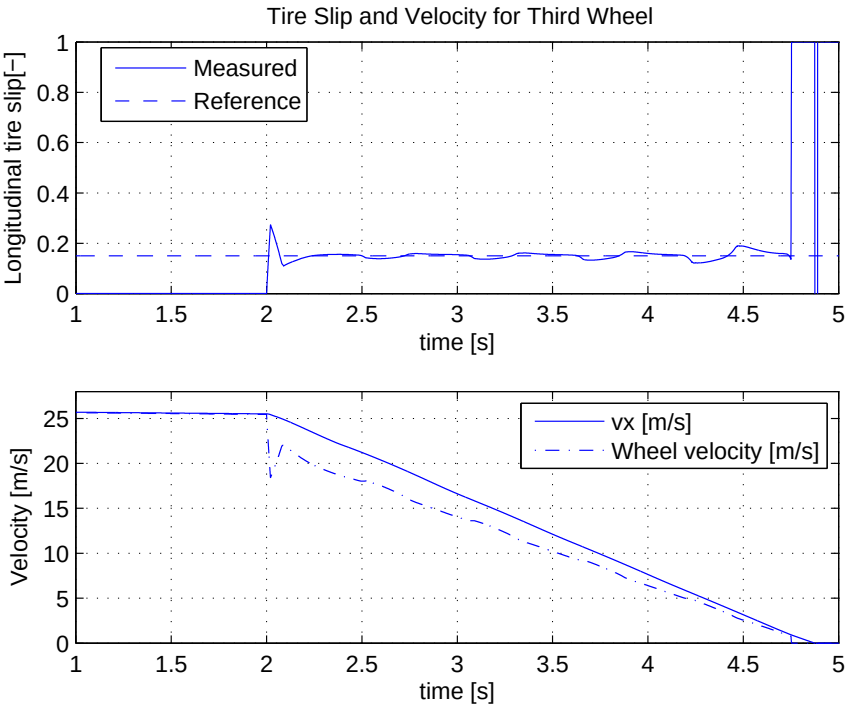

Figure 4.1 Tire slip, denoted 'measured', and longitudinal velocity versus time during an ABS braking with $\mu = 1$ and a reference slip of 0.15. The ABS is activated when the slip due to emergency braking goes above some given threshold, in this case $\lambda = 0.15$, and because of that there is an overshoot in the beginning.

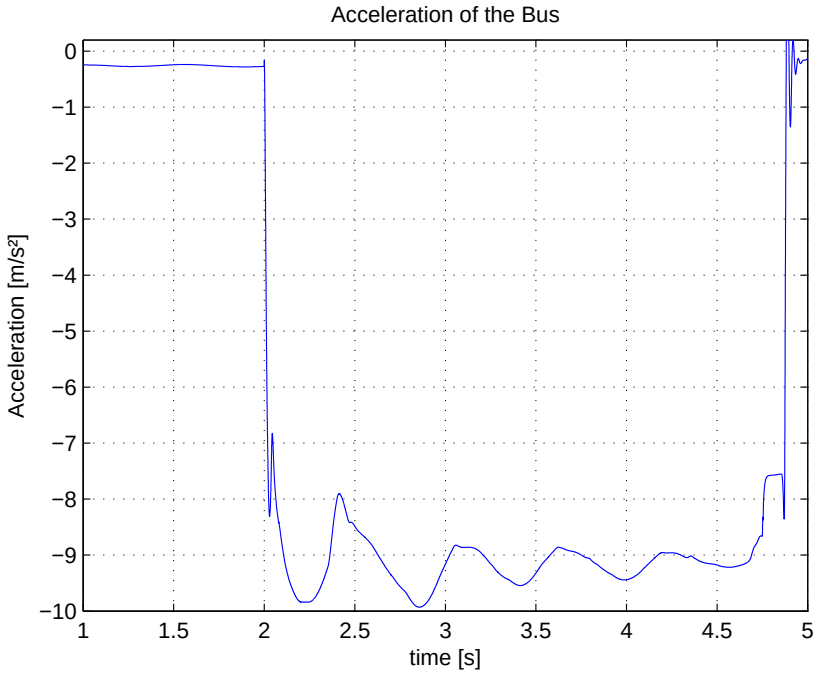

Figure 4.2 Acceleration versus time during an ABS braking with $\mu = 1$. The theoretical maximum is the gravitational constant times the friction coefficient, in this case about 9.8 m/s^2.

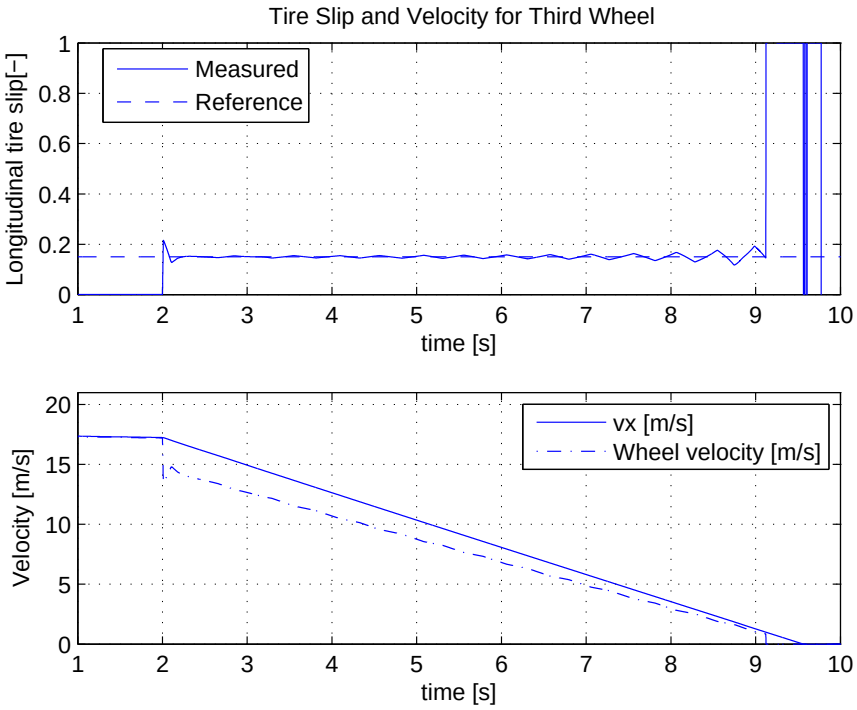

Figure 4.3 Tire slip and velocity during an ABS braking on a road with $\mu = 0.3$, and a reference slip of 0.15.

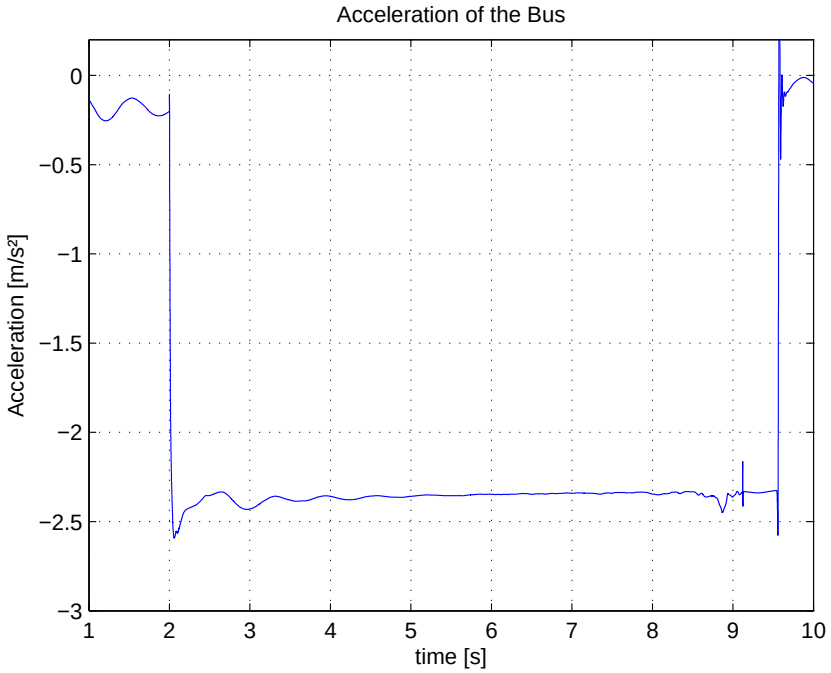

Figure 4.4 Acceleration during an ABS braking. The theoretical maximum is the gravitational constant times the friction coefficient, in this case about 3 m/s^2. The acceleration is in this case not as close to the theoretical maximum as for $\mu = 1$, and that because the reference value is the same as the one which generates maximum force for $\mu = 1$.

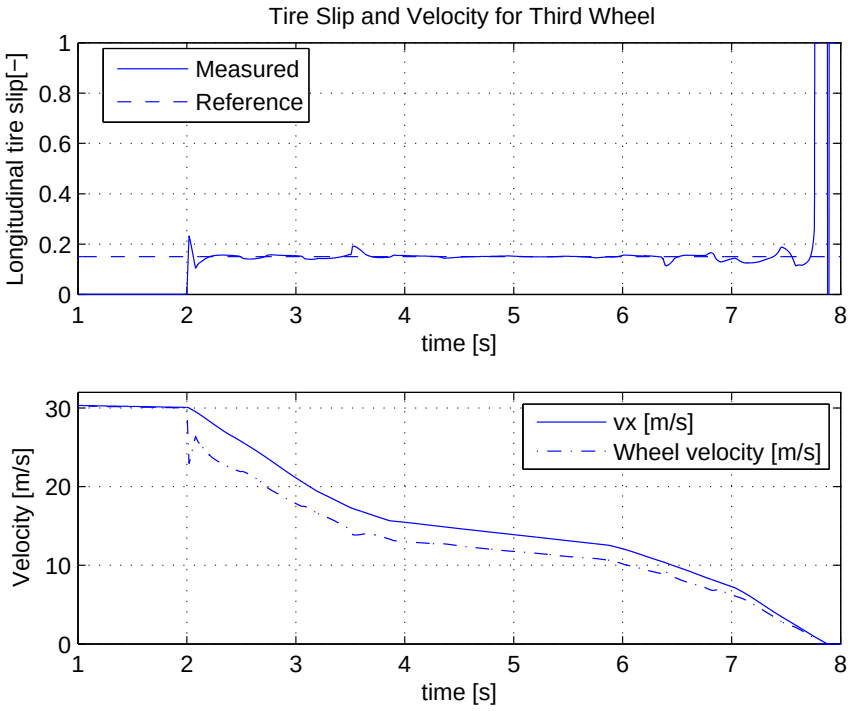

Figure 4.5 A plot showing tire slip and velocity during an ABS μ-step braking with a reference slip of 0.15.

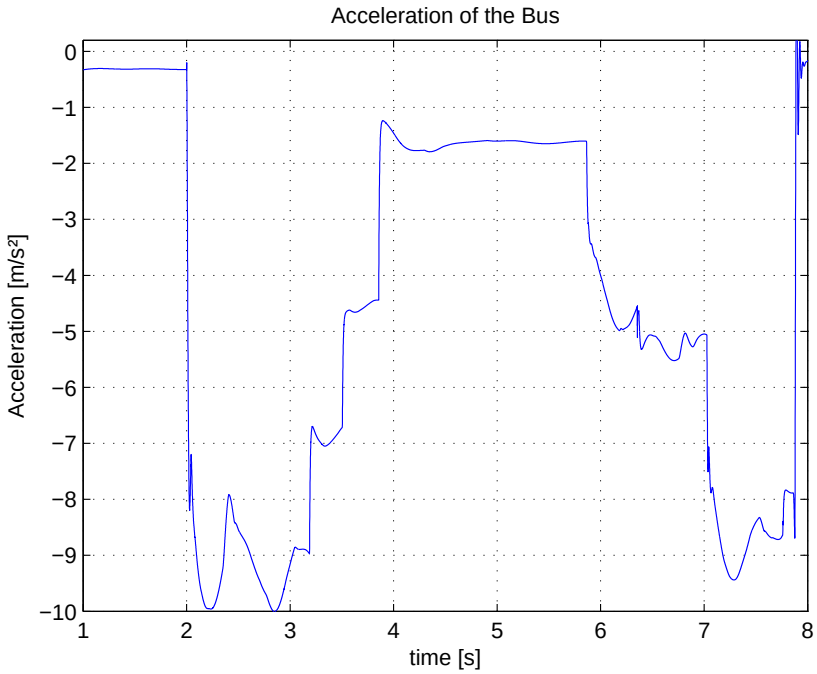

Figure 4.6 Acceleration during an ABS μ-step braking.

4.2 Discussion

The controller is seen to work well, with the performance being consistent under a wide range of conditions. One problem with the controller is the performance at low speed where the slip oscillates more, which was to be expected from the analysis in Section 3.1. This can be avoided by letting the target slip increase slowly when the velocity decreases. Although only one reference slip is shown in the plots, tests carried out have validated that the controller works for all slip values.

The results for the other wheels are similar, even though the controller works somewhat worse for the wheels on the front axle. This is to be expected according to the longitudinal load transfer model in Section 2.8, where the forces due to load transfer are given by (2.18)-(2.20). It can be observed from those equations that the front axle will exhibit more load transfer than the two other axles, which makes it harder to control the slip since the dynamics changes more than for the other wheels. The simulation results for the other axles are, as mentioned earlier, shown in Section B.1.

Despite the fact that the simulator used is very advanced, performance in a real bus might differ due to noise in measurements/estimations, unmodeled dynamics and additional time delays.

4.3 Evaluation of the ASR

Since the bus is not capable of making the wheels spin at friction values approximately higher than $\mu = 0.3$, all tests were carried out with the friction coefficient set to 0.2. Two different types of tests were done, and are described below:

1. Low μ. After a couple of seconds of steady state driving the driver suddenly pushes the acceleration pedal to give full engine torque.
2. μ-step. Full acceleration starts on a high friction road where suddenly a low friction surface is encountered. After a couple of seconds the road has again high friction.

The plots shown will be of the fifth wheel, but the results for the sixth wheel are of course the same due to symmetry.

Low μ

As observed from Figure 4.7, the controller catches the slip when the wheels are about to spin and controls it smoothly around $\lambda = -0.15$.

μ-Step

Also here the performance is good, as seen in Figure 4.8. The rapid change of surface constitutes no problem for the controller.

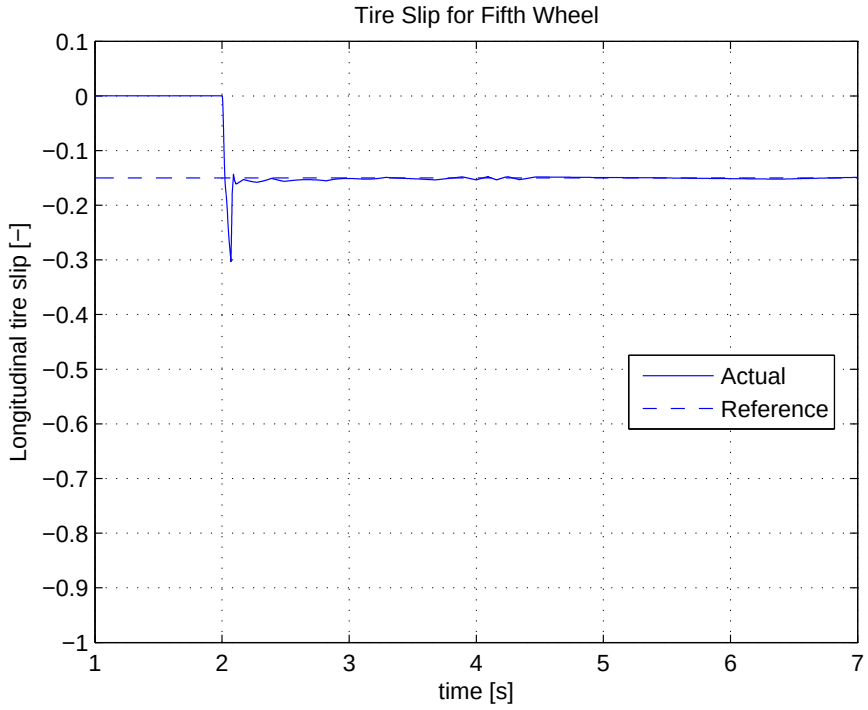

Figure 4.7 Tire slip versus time during a full acceleration on a $\mu = 0.2$ surface with a reference slip of -0.15.

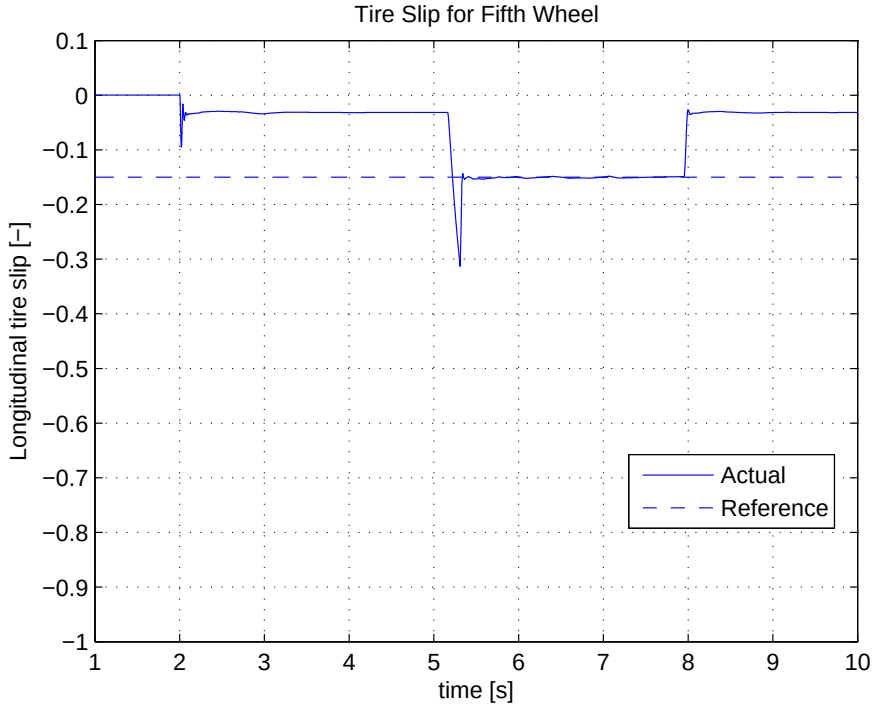

Figure 4.8 Tire slip versus time during a full acceleration on a μ-step surface with a reference slip of -0.15. The ASR is turned on at approximately 5 seconds.

4.4 Discussion

The controller performs well. Since the use of the ASR in this thesis is not as extensive in the ESP as the ABS, the control parameters were not tuned as carefully. The performance is still very good, with smooth following of the reference.

5. Yaw Rate Control Design

This chapter develops the remainder of the ESP, taking advantage of the previously designed ABS. This is a natural solution due to the brakes being standard equipment. This is, however, not the only solution; several researchers have used the Steer-by-wire [Rajamani, 2006] concept with promising results in simulation.

The goal of the ESP is to monitor the lateral movement of the vehicle and intervene when a critical situation arises. A critical situation is here excessive understeering or oversteering. Understeering is when the front wheels produce too small lateral forces, and as a result the vehicle steers with a radius of curvature larger than desired. Oversteering is when the vehicle drives with a radius of curvature smaller than desired, which happens because of saturation of the lateral forces of the rear wheels.

The sensors used are a steering wheel angle sensor, a lateral acceleration sensor, a yaw rate sensor and wheel speed sensors for estimation of the longitudinal velocity. It should be noted that the sensors for lateral acceleration and yaw rate are assumed to measure these quantities for the front part of the bus.

The controller can be seen as divided into two parts. One part calculates a desired torque to stabilize the vehicle, and the other part distributes this torque out to appropriate wheels. The situation is shown in Figure 5.1. The total moment coming from the upper controller is sent as an input to the lower controller, which calculates a desired slip for each wheel on the front part of the bus. This reference slip is sent to the ABS, which produces a corresponding brake pressure.

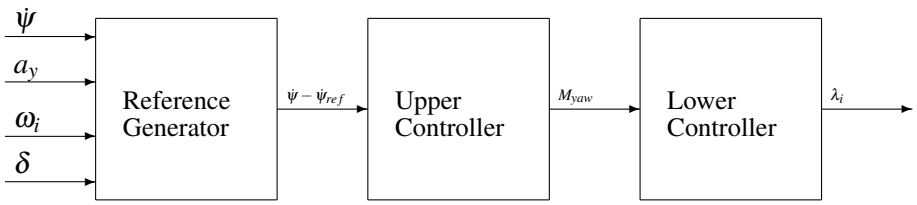

Figure 5.1 The control structure of the ESP. One of the controllers calculates the desired torque, and the other part tries to distribute this torque out to the wheels by sending the calculated reference slip for each wheel to the ABS.

5.1 Upper Controller

As said before, the upper controller calculates a desired moment to stabilize the bus. This is done based on the difference between the measured yaw rate of the front part of the bus and some generated reference yaw rate. The sideslip angle β must also be limited to prevent spin-out, but this quantity can be controlled indirectly via the yaw rate. In fact, β is most often not estimated in vehicles, and thus it can not be controlled explicitly.

A common method to calculate a torque to stabilize the vehicle through the yaw rate is to use a P(I)(D)-controller [Isermann, 2006]. This is a convenient solution because for a regular car the dynamics for the yaw rate is, which can be seen from

(2.44) and by setting $F_{y,p} = 0$,

$$\ddot{\psi} = \frac{M}{I_{zz}}.$$

Here, M denotes the moment the wheels give rise to. The transfer function of this system is a pure integrator, which makes it sufficient to use a P-controller.

There are also other attempts of controllers. In [Eisele and Peng, 2000] two P-controllers are used to simultaneously control yaw rate and sideslip angle of a tractor-trailer combination. In [Rajamani, 2006], a Lyapunov based *sliding mode* controller is used to control the yaw rate and the sideslip angle. The longitudinal forces are seen as inputs to the system and the lateral forces are estimated with the HSRI Tire Model presented in Section 2.2. Those approaches demand high quality measurements or estimations of β, something which is not available.

The model (2.43) derived in Chapter 3 can be used to try to design a controller for the yaw rate. This model is, however, derived under the assumption of stable driving conditions and can therefore be misleading if one for example tries to design a controller by pole placement, or any other linear method for that matter.

Because it is desired to keep the controller as simple as possible the choice of a simple controller, for example a P-controller, looks tempting. Surely, it would be possible to eliminate the nonlinear dynamics coming from the trailer by including an integral part and performing trial and error tuning of the controller gain. Due to the reason that it is better to do some kind of stability analysis of the controller, Lyapunov theory will be used for the control design.

Lyapunov Theory

As with the case of the Circle Criterion, Lyapunov theory is often used to prove stability of the nonlinear system considered. The reader is referred to [Khalil, 2000] for proofs and more in-depth reading about Lyapunov and sliding mode theory.

Time Invariant Systems Consider the system

$$\dot{x} = f(x) \tag{5.1}$$

where $f : D \to \mathbf{R}^n$ is a locally Lipschitz map from a domain $D \subset \mathbf{R}^n$ into $\mathbf{R}^n$.

This system is said to be autonomous. In practice it means that it is not explicitly dependent on time.

DEFINITION 5.1
The equilibrium point $x = 0$ of (5.1) is

- stable, if for each $\varepsilon > 0$ there exists $\delta = \delta(\varepsilon) > 0$ such that

$$||x(0)|| < \delta \implies ||x(t)|| < \varepsilon, \quad \forall t \geq 0.$$

- unstable if it is not stable.
- asymptotically stable if it is stable and δ can be chosen such that

$$||x(0)|| < \delta \implies \lim_{t \to \infty} x(t) = 0.$$

□

The following theorem shows how to prove stability of a general system without solving any differential equations.

THEOREM 5.1
Let $x = 0$ be an equilibrium point for (5.1) Let $V : \mathbf{R}^n \to \mathbf{R}$ be a continously differentiable function such that

- $V(0) = 0$
- $V(x) > 0, \quad \forall x \neq 0$
- $\dot{V} \leq 0$
- $||x(0)|| \to \infty \implies V(x) \to \infty$

then $x = 0$ is a globally stable equilibrium point for (5.1). If the above only holds for some smaller region $\Omega \in \mathbf{R}^n$, then $x = 0$ is said to be locally stable. If the conditions are strenghtened to also include $\dot{V} < 0$, then $x = 0$ is said to be locally/globally asymptotically stable. □

The assumption of an equilibrium point at the origin is no restriction since if the system $\dot{x} = f(x)$ has an equilibrium point at $x_0 \neq 0$, the system can be shifted with the change of variables $y = x - x_0$ as

$$\dot{y} = \dot{x} = f(x) = f(y + x_0) \equiv g(y), \text{ where } g(0) = 0,$$

similar to the case with the circle criterion before.

Time Varying Systems When the system is explicitly dependent on time, it is said to be nonautonomous. The corresponding definitions and theorems are cited below.

Consider the system

$$\dot{x} = f(t, x) \tag{5.2}$$

where $f : [0, \infty) \times D \to \mathbf{R}^n$ is piecewise continous in t and locally Lipschitz in x on $D : [0, \infty) \times D$, and $D \subset \mathbf{R}^n$ is a domain that contains the origin $x = 0$. If

$$f(t, 0) = 0, \quad \forall t \geq 0,$$

then the origin is an equilibrium point of (5.2).

The following definition has been stated in Chapter 3 already, but is restated for convenience.

DEFINITION 5.2
The equilibrium point $x = 0$ of (5.2) is

- stable if, for each $\varepsilon > 0$, there is $\delta = \delta(\varepsilon, t_0) > 0$ such that

$$||x(t_0)|| < \delta \implies ||x(t)|| < \varepsilon, \quad \forall t \geq t_0 \geq 0. \tag{5.3}$$

- uniformly stable if, for each $\varepsilon > 0$, there is $\delta = \delta(\varepsilon) > 0$, independent of t_0, such that (5.3) is satisfied.
- unstable if it is not stable.
- asymptotically stable if it is stable and there is a positive constant $c = c(t_0)$ such that $x(t) \to 0$ as $t \to \infty$, for all $||x(t_0)|| < c$.
- uniformly asymptotically stable if it is uniformly stable and there is a positive constant c, independent of t_0, such that for all $||x(t_0)|| < c$, $x(t) \to 0$ as $t \to \infty$, uniformly in t_0; that is, for each $\nu > 0$, there is $T = T(\nu) > 0$ such that

$$||x(t)|| < \nu, \quad \forall t \geq t_0 + T(\nu), \ \forall ||x(t_0)|| < c.$$

- globally uniformly asymptotically stable if it is uniformly stable, $\delta(\varepsilon)$ can be chosen to satisfy $\lim_{\varepsilon\to\infty}\delta(\varepsilon)=\infty$ and for each pair of positive numbers ν and c, there is $T=T(\nu,c)>0$ such that

$$||x(t)||<\nu,\quad \forall t\geq t_0+T(\nu,c),\ \forall||x(t_0)||<c.$$

□

The following Theorem is a nonautonomous variant of Theorem 5.1.

THEOREM 5.2
Let $x=0$ be an equilibrium point for (5.2) and $D\subset\mathbf{R}^n$ be a domain containing $x=0$. Let $V:[0,\infty)\times D\to\mathbf{R}$ be a continously differentiable function such that

$$W_1(x)\leq V(t,x)\leq W_2(x), \tag{5.4}$$

$$\frac{\partial V}{\partial t}+\frac{\partial V}{\partial x}f(t,x)\leq 0, \tag{5.5}$$

$\forall t\geq 0$ and $\forall x\in D$, where $W_1(x)$ and $W_2(x)$ are continous positive definite functions on D. Then $x=0$ is uniformly stable. Assume that the above holds with (5.5) strenghtened to

$$\frac{\partial V}{\partial t}+\frac{\partial V}{\partial x}f(t,x)\leq W_3(x)$$

where $W_3(x)$ is a continous negative definite function on D. Then $x=0$ is uniformly asymptotically stable. □

Just as in the case of autonomous systems, it is no restriction to consider equilibrium points at the origin. Furthermore, a *nonzero solution* of (5.2) can also be translated to the origin. To see this, assume that $y_0(\tau)$ is a solution of the system

$$\frac{dy}{d\tau}=g(\tau,y)$$

defined for all $\tau\geq a$. Introduce the change of variables

$$x=y-y_0(\tau);\ t=\tau-a.$$

This transforms the system into

$$\dot{x}=g(\tau,y)-\dot{y}_0(\tau)=g(t+a,x+y_0(t+a))-\dot{y}_0(t+a)\equiv f(t,x).$$

Since

$$\dot{y}_0(t+a)=g(t+a,x+y_0(t+a)),\quad \forall t\geq 0,$$

the origin $x=0$ is an equilibrium point of the transformed system at $t=0$. This means that if $y_0(\tau)$ is not constant, the transformed system will be time-dependent even when the original system is not. Therefore stability for time varying equilibrium points must be discussed in the context of nonautonomous systems.

Since the reference yaw rate will be changing with time, there is a need in this case for using the theory considered in this section, although the dynamics of (2.45) is nonautonomous.

Control Design

The aim of the design is to make the yaw rate follow a specified reference. There are a number of different candidates for a Lyapunov function able to show convergence. In [Rajamani, 2006] a suitable Lyapunov function is chosen as $V = \frac{1}{2}\Big((\dot{\psi} - \dot{\psi}_{ref})^2 + \xi(\beta - \beta_{ref})^2\Big)$, where ξ is a weighting factor.

Consider the function above with $\xi = 0$ as the Lyapunov function candidate

$$V(x,t) = \frac{1}{2}(\dot{\psi} - \dot{\psi}_{ref})^2 = \frac{1}{2}\sigma^2.$$

The time derivative of $V(x,t)$ is

$$\dot{V} = \frac{\partial V}{\partial t} + \frac{\partial V}{\partial \dot{\psi}}\ddot{\psi} = -\sigma\ddot{\psi}_{ref} + \sigma\ddot{\psi}. \tag{5.6}$$

The dynamics from (2.45) is inserted into (5.6), and thus the derivative becomes

$$\begin{aligned}
\dot{V} &= \sigma(-\ddot{\psi}_{ref} + \ddot{\psi}) \\
&= \sigma\Bigg(-\ddot{\psi}_{ref} + \frac{1}{I_{zz1}}\Big(F_{y1}(l_f\cos\delta + y_f\sin\delta) + F_{x1}(y_f\cos\delta - l_f\sin\delta) \\
&+ F_{y2}(l_f\cos\delta - y_f\sin\delta) - F_{x2}(y_f\cos\delta + l_f\sin\delta) \\
&- l_m F_{y3} + y_m F_{x3} - (l_m F_{y4} + y_m F_{x4}) - x_2 F_{yp}\Big)\Bigg) \\
&= \sigma\left(\frac{M_{yaw} - x_2 F_{yp}}{I_{zz1}} - \ddot{\psi}_{ref}\right).
\end{aligned} \tag{5.7}$$

By introducing the signum function as

$$sign(x) = \begin{cases} 1 & \text{if } x > 0 \\ 0 & \text{if } x = 0 \\ -1 & \text{if } x < 0 \end{cases}$$

and setting

$$M_{yaw} = I_{zz1}(\ddot{\psi}_{ref} - \eta\, sign(\sigma)),$$

the derivative of $V(t,x)$ becomes

$$\dot{V} = \sigma\left(-\eta\, sign(\sigma) + \frac{x_2 F_{yp}}{I_{zz1}}\right) \leq 0 \text{ if } \eta > \frac{x_2 F_{yp}}{I_{zz1}}.$$

Here F_{yp} is of course not measurable, but from a torque balance around the center of gravity of the trailer a rough estimate can be found quickly. The estimated η is then adjusted to give desired performance.

With the Lyapunov function

$$V(x,t) = \frac{1}{2}(\dot{\psi} - \dot{\psi}_{ref})^2 = \frac{1}{2}\sigma^2$$

and Theorem 5.2, it is concluded that the control law $M_{yaw} = I_{zz1}(\ddot{\psi}_{ref} - \eta\, sign(\sigma))$ renders the solution $\dot{\psi}_0 = \dot{\psi}_{ref}$ uniformly asymptotically stable, as long as η is large enough.

Implementational Aspects

Since the signum function in practise leads to extreme high-gain control, it is often modified. In [Khalil, 2000] the signum function is approximated as

$$sign(x) \approx sat(\frac{x}{\varepsilon}),$$

where $sat(x)$ is equal to x if $|x| \leq 1$ and ± 1 otherwise. The functions are shown in Figure 5.2. This will have an impact on the stability of the controller. However, in the

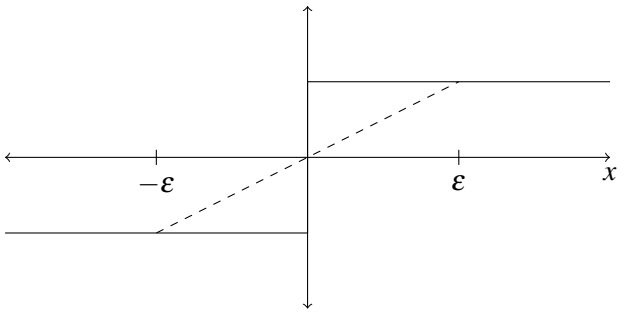

Figure 5.2 The signum function, the solid line, and the saturation function, the dashed line. The lower ε is, the more accurate is the approximation.

region where $sat(\frac{x}{\varepsilon}) = \pm 1$ the saturation and signum functions are equal, and therefore with this approximation it is ensured that $\dot{\psi}$ will in a worst case only converge to a region ε away from the equilibrium point. Of course, simulations will give a suitable ε to use.[1]

Yaw Rate Reference Generation

The question now is how to generate a desired yaw rate for the controller. In [Tøndel and Johansen, 2005] a yaw rate reference in case of oversteering is defined as

$$\dot{\psi}_{ref} = \begin{cases} \dot{\psi} & \text{if } |\dot{\psi}| \leq \dot{\psi}_{max} \\ \pm\dot{\psi}_{max} & \text{if } |\dot{\psi}| \geq \dot{\psi}_{max} \end{cases}$$

This means that the controller only interacts when the yaw rate goes above some defined $\dot{\psi}_{max}$. In [Kiencke and Nielsen, 2005] the above method of reference generation is originally used, together with the following condition for understeering,

$$\dot{\psi}_{ref} = \begin{cases} \dot{\psi} & \text{if } |\alpha_f/\alpha_r| \leq c \\ \pm\dot{\psi}_{max} & \text{if } |\alpha_f/\alpha_r| > c \end{cases}$$

Here c is normally a value in the range of 1.5-2.5. In both [Isermann, 2006] and [Rajamani, 2006] a simplified linear one-track model is used to generate the reference. The linear one-track model is on the form

$$\dot{x} = Ax + Bu,$$

where x is a vector containing $\dot{\psi}$ and v_y and $u = \delta$. A and B are matrices of suitable size. By putting $\dot{x} = 0$ and solving for the yaw rate one gets a linear dependency

[1] This approximation also removes the theoretical issues with the discontinuity of the controller, which hinders the state equation (5.2) from being locally Lipschitz at $\dot{\psi} = \dot{\psi}_{ref}$.

between ψ and δ. This is the simplified one-track model. In [Eisele and Peng, 2000], where the goal is to control a tractor-trailer combination, a dependency between the steering angle required to produce a steady state yaw rate for the tractor at a given velocity is verified by experiments. Then a reference yaw rate can be produced as $\dot{\psi}_{ref} = (av_x + b)\delta$, where a and b are constants to be determined.

As seen from the above examples, the model does not need to be complicated. The only requirement is that the model follows the real vehicle during steady state maneuvers so that the ESP is not triggered excessively. Motivated by this, (2.46) is taken to produce the desired yaw rate in this thesis. There are, however, modifications that need to be done in order for the model to work properly. Some of these may be found in [Isermann, 2006].

Implementational Modifications of Reference Model The model chosen to produce a reference yaw rate is (2.46) on page 24 which is repeated below.

$$\begin{pmatrix} \dot{v}_{y1} \\ \ddot{\psi}_1 \end{pmatrix} = \begin{pmatrix} -\frac{C_{\alpha_f}+C_{\alpha_m}}{m_1 v_{x1}} & \frac{l_m C_{\alpha_m} - l_f C_{\alpha_f}}{m_1 v_{x1}} - v_{x1} \\ \frac{l_m C_{\alpha_m} - l_f C_{\alpha_f}}{I_{zz1} v_{x1}} & -\frac{l_f^2 C_{\alpha_f} + l_m^2 C_{\alpha_m}}{I_{zz1} v_{x1}} \end{pmatrix} \begin{pmatrix} v_{y1} \\ \dot{\psi}_1 \end{pmatrix} + \begin{pmatrix} \frac{C_{\alpha_f}}{m_1} \\ \frac{l_f C_{\alpha_f}}{I_{zz1}} \end{pmatrix} \delta$$

The first modification that needs to be done is due to that the steering angle of the wheels can not be measured, so the measured steering angle at the steering wheel must be translated to a steering angle for the wheels. This is done by measuring the steady state relationship between the steering wheel angle and the angle of the wheels, which is then implemented as a look-up table.

One of the assumptions when deriving the model was a constant longitudinal velocity. This is, of course, not generally the case during extreme cornering, and therefore the system will be fed with both v_{x1} and δ.

Another assumption was a linear dependence between the lateral force and the sideslip angle α. During extreme cornering the lateral forces saturate although the forces of the reference model do not, so the output of the reference model has to be limited: The relationship

$$a_y = \dot{v}_y + v_x \dot{\psi} \tag{5.8}$$

holds. There is also the previously defined formula

$$\frac{v_y}{v_x} = \tan\beta.$$

By moving over v_x, differentiating and inserting the result into (5.8), a_y is expressed as

$$a_y = v_x \dot{\psi} + \dot{v}_x \tan\beta + \frac{v_x \dot{\beta}}{\sqrt{1 + (\tan\beta)^2}}. \tag{5.9}$$

Since the goal is to keep β small and smooth, the first expression in (5.9) dominates. This leads to the relation $a_y \approx v_x \dot{\psi}$, and hence the reference yaw rate must be bounded as

$$|\dot{\psi}_{ref}| \leq \left| \frac{a_y}{v_x} \right|. \tag{5.10}$$

The reference yaw rate in this thesis is therefore produced as:

$$\dot{\psi}_{ref} = \begin{cases} \dot{\psi}_{ref} & \text{if } |\dot{\psi}_{ref}| \leq \left|\frac{a_{y1}}{v_{x1}}\right| \\ \pm \left|\frac{a_{y1}}{v_{x1}}\right| & \text{if } |\dot{\psi}_{ref}| \geq \left|\frac{a_{y1}}{v_{x1}}\right| \end{cases}$$

The ESP will not intervene immediately when the yaw rate deviates from the desired one. If the ESP would intervene immediately when the yaw rate goes above the reference, it would from (5.9) and (5.10) correspond to the assumption that a desired value of the sideslip angle $\beta = 0$. When the driver performs a maneuver that triggers the ESP, it is instead probable that a desired β is slightly larger than zero. This is the same as letting the yaw rate go above the defined maximum reference with a fairly small amount. The deviation then corresponds to how large vehicle sideslip angle is allowed.

When the bus is understeering it is more probable that it is stable[2] than when the bus is oversteering. Therefore the bus is allowed to understeer more than it is to oversteer. Some suitable limits for the allowed deviation was found to be 3 deg/s for oversteering and 5 deg/s for understeering. The ESP is in this thesis turned off when the error becomes smaller than 1 deg/s to avoid chattering in yaw rate and brake pressures.

5.2 Lower Controller

The goal of the lower controller is to allocate the desired torque out to the wheels. For a regular car, this is in [Isermann, 2006] done by braking the front outer wheel in case of oversteering and the rear inner wheel during understeering. In [Eisele and Peng, 2000] a tractor and trailer combination is stabilized by braking the outer wheels on the front tractor and trailer axles during oversteering and the wheel on the rear trailer axle if understeering.

One has to be careful when braking the rear wheels of the front part in an oversteering situation, because as pointed out in Section 2.2 the lateral forces decrease when the longitudinal forces are increased. This will lead to the rear outer wheel losing some of its side force. The net effect on the torque will at first be positive because the longitudinal force increases very fast for low slip values. When the longitudinal slip grows the gradient of the longitudinal force will be smaller, while the side force will start to decrease even faster. This will eventually lead to a destabilizing effect[3]. For an articulated vehicle this also implies an increased risk of jackknifing. This means that if one is to use the rear tractor wheels during oversteering, only a small amount of the desired torque should be allocated to this wheel. The same reasoning apply for the front inner wheel during understeering. In fact, it can be shown that the optimal, in terms of achieving the desired moment, allocation for oversteering is to brake the rear outer wheel so that it follows a low reference slip [Tøndel and Johansen, 2005]. The situation for oversteering is shown in Figure 5.3.

Reference Slip Generation

In this thesis the wheels to brake are in case of oversteering taken to be the tractor outer wheels plus both trailer wheels. In case of understeering the wheels to brake are the inner wheels of the tractor. The reason for braking the trailer wheels when the bus oversteers is that the trailer otherwise will "push" the tractor even more into oversteering, potentially leading to jackknifing. By slowing down the bus somewhat this effect is lowered. When the bus is understeering there is a desire from the controller to increase the yaw rate, and therefore the trailer wheels are not used in this case.

[2] This is because the vehicle sideslip angle is fairly small in this case, and as discussed earlier several implementations do not intervene at all during understeering.

[3] The value of the longitudinal slip when this happens is different for different types of vehicles, but is typically between 5-10 degrees.

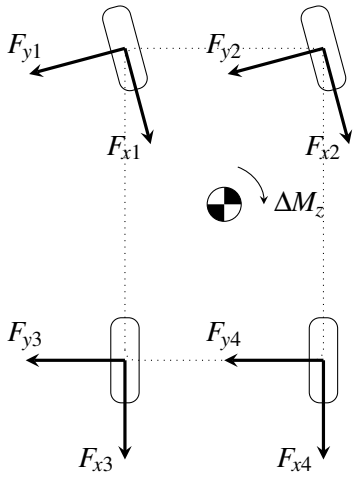

Figure 5.3 A situation showing the forces from the wheels during cornering. If the purpose is to avoid oversteer the outer rear wheel may also be used for braking. However, if the longitudinal slip grows too large the lateral force on the fourth wheel will vanish and the vehicle will start to oversteer even more. This is of course not desirable.

Trailer Wheels For the trailer wheels a reference slip of $\lambda_{ref} = 0.04$ is set immediately when the controller is activated, enough to slow down the bus somewhat. When the yaw rate error grows larger than 6 deg/s an additional reference slip of 0.03 is added. These reference changes are made dynamically with a small time constant for comfort reasons.

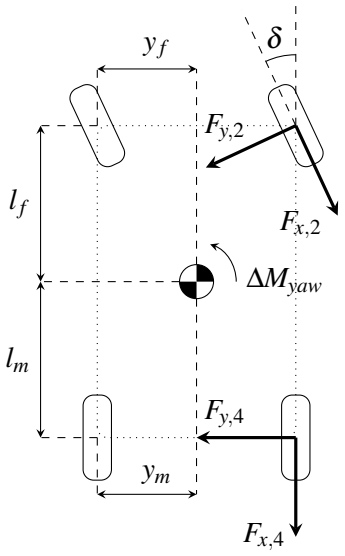

Figure 5.4 An oversteer situation where the ESP will stabilize with the outer front and rear wheel on the tractor.

Tractor Wheels Assume an oversteer situation as in Figure 5.4, where the ESP will try to stabilize the tractor with the outer front and rear wheels. Let the desired change

in moment be denoted ΔM_{yaw}. Then differentiation gives that

$$\begin{aligned}\Delta M_{yaw} &= \frac{\partial M_{yaw}}{\partial \lambda_2} \cdot \Delta\lambda_2 + \frac{\partial M_{yaw}}{\partial \lambda_4} \cdot \Delta\lambda_4 \\ &= \frac{\partial F_{y,2}}{\partial \lambda_2} \cdot \Delta\lambda_2 (l_f \cos\delta - y_f \sin\delta) \\ &\quad - \frac{\partial F_{x,2}}{\partial \lambda_2} \cdot \Delta\lambda_2 (y_f \cos\delta + l_f \sin\delta) \\ &\quad - \frac{\partial F_{y,4}}{\partial \lambda_4} \cdot \Delta\lambda_4 l_m - \frac{\partial F_{x,4}}{\partial \lambda_4} \cdot \Delta\lambda_4 y_m, \end{aligned} \tag{5.11}$$

where the forces are defined positive as in Figure 5.4. By adding constants it is possible to decide which wheel will have the greatest impact on the torque. This is done as

$$\Delta M_{yaw} = k_s \frac{\partial M_{yaw}}{\partial \lambda_2} \cdot \Delta\lambda_2 + (1-k_s) \frac{\partial M_{yaw}}{\partial \lambda_4} \cdot \Delta\lambda_4. \tag{5.12}$$

It is straightforward to do this derivation for the other situations as well. From (5.12) the change in slip that is required to produce a desired torque may be calculated if a suitable model for the forces is used.

The ESP will only intervene when the bus is at the stability limits. Thus it is appropriate to assume that the forces saturate, which motivates the use of the Kamm-circle to model the forces. The equations are restated for convenience:

$$\begin{aligned} F_x &= \frac{\lambda}{\sqrt{\lambda^2+\alpha^2}} \cdot \mu F_z \\ F_y &= \frac{\alpha}{\sqrt{\lambda^2+\alpha^2}} \cdot \mu F_z \end{aligned}$$

These equations, after differentiation, are inserted into (5.11) and the reference slip may then be calculated.

In these equations neither the maximum friction coefficient nor the normal forces that the load gives rise to are known, and must therefore be estimated. The load that rests on each wheel may be calculated with the load transfer model derived in Section 2.4. Because the lateral acceleration is much larger than the longitudinal, only lateral load transfer is used in this thesis. The mass can be taken from the fully loaded bus, the empty bus or a compromise between these two. For this thesis the mass is taken to be that of the loaded bus.

The maximum achievable acceleration at center of mass is for physical reasons limited by

$$\sqrt{a_y^2 + a_x^2} \leq \mu g.$$

Because of the assumption that α is large enough for the lateral forces to saturate, the relation

$$a_y \approx \mu g$$

holds before braking is started. From (2.21) on page 16, the longitudinal acceleration can be written as

$$a_x = \dot{v}_x - v_y \dot{\psi}. \tag{5.13}$$

In some cars and buses a_x is measured, but in this thesis that is not considered a certainty, so the following reasoning is instead used: In (5.13) the first term is much

larger than the second if β is small. Then the longitudinal acceleration can be approximated as $a_x \approx \dot{v}_x$. This quantity is not measurable, so it must be estimated. In this thesis the estimation is performed as

$$\dot{v}_x(t) \approx \frac{v_x(t) - v_x(t - T_s)}{T_s}. \tag{5.14}$$

A rough estimate of the coefficient of friction is then taken to be

$$\mu = \frac{\sqrt{a_y^2 + \dot{v}_x^2}}{g}$$

with (5.14) inserted, which will be accurate enough for the purpose in this thesis. For more advanced friction estimation, the reader is referred to [Schofield, 2008] and [Svendenius, 2007].

The maximum allowed reference slip is set to 0.7 since if a wheel is allowed to lock, it will make the lateral force of the wheel vanish completely with no steerability left for the driver. The derivation of the desired reference slip as a function of the desired change in moment, resulting in (5.12), takes into account that the moment of the rear outer and front inner tractor wheels are only stabilizing the yaw rate up to a certain slip. However, model uncertainties in the Kamm-circle model, the friction coefficient and the loading conditions make it important that the reference slip is saturated for these wheels. In an oversteer situation the reference slip for the outer rear wheel on the tractor may not exceed 0.05. The limit 0.08 is taken for the inner front wheel in case of understeering. The difference between these two limits has to do with the position of center of mass. The limits are not reached often because of the reasons mentioned above, but they are still set as a precaution.

5.3 Summary

In this chapter the design of the ESP has been concluded. The proposed yaw rate controller is rather simple, with the motivation being the dynamics of the yaw rate. The high-gain properties of the controller ensures that it is robust to unmodeled dynamics present, for example due to roll of the vehicle.

The yaw rate generation is done with a saturated linear one-track model. The important part of the reference generator is to follow the vehicle in a reasonable way during steady state maneuvers so that the controller is not triggered when it is not necessary. Another, probably more accurate, option would be to use (2.43) for reference generation.

The Kamm-circle is used to model the forces and to produce a desired reference slip. This model gives a good fit of the forces during extreme maneuvering. To estimate the load on each wheel the load transfer model derived in Section 2.4 is used.

As shown in the chapter, one has to be careful when choosing the wheels to brake and how much. This is even more important for articulated vehicles, which has been discussed briefly.

6. Evaluation of the ESP

In this chapter, the result of the ESP is shown together with some plots of the bus with no control system at all. The first part of the chapter deals with stabilization at low velocities, where as the second part is concerned with low velocity maneuvers.

Obviously, it is both easier and less expensive to have as few different safety algorithms in the bus as possible. The best would be if the ESP is capable of keeping the bus stable on its own, so that a separate controller for the link is not needed. The simulations shown will hopefully make it clear whether this is the case or not.

To validate the ESP and find some possible drawbacks in its performance, several maneuvers were tested at different velocities and road conditions. The results for the so called fishhook and J-turn maneuvers will be presented here. These maneuvers were primarily used because they are the most standard maneuvers when investigating vehicle stability and force the vehicle to its physical limits. The simulation results in the report are considered to give a good picture of the overall performance that can be expected from the ESP for other maneuvers as well.

As with the ABS and the ASR evaluation, the performance in a real bus will probably not be the same due to for example noise in measurements and estimations. Still, the high degree of realism of the simulator ensures real-like results.

6.1 Stability Conditions

In order to decide whether the bus is considered to be stable or unstable during a maneuver, some conditions have to be determined. For example, the bus can be considered unstable if the articulation angle grows beyond what is reasonable or if the bus jackknifes. This is because the driver of the bus is then not able to influence the direction of it. Another stability condition is that the yaw rate must not grow too large and oscillate, because this is a sign that the bus is rotating in an uncontrolled way. In short one can say that the yaw rate is allowed to be larger the slower the vehicle speed is. From the simulations it will hopefully be clear when the yaw rate is stable or not.

The sideslip angle is the most important measure to see if the bus is steerable or not. A large sideslip angle means that the lateral velocity compared to the longitudinal is not small, which is because of the relationship

$$\tan\beta = \frac{v_y}{v_x}$$

defined in Chapter 3. A high lateral velocity indicates that the bus is skidding, and that is of course not good for the steerability of the bus. In [Kiencke and Nielsen, 2005], a maximum allowed sideslip angle is defined as

$$\beta_{max} = 10 - 7\frac{v_x^2 + v_y^2}{40^2}, \tag{6.1}$$

where the limit is defined in degrees and the velocity in m/s. If the sideslip angle grows beyond this limit the bus can be considered unstable. In [Liebemann *et al.*, 2005], a limit where a vehicle's steerability vanish is determined to be 4 degrees on snow and about 10 degrees on dry asphalt. To combine these two conditions one can multiply the limit for β_{max} with the coefficient of friction to account for lower allowed

sideslip angles at low friction. In any case, during everyday driving on dry roads, a driver rarely experiences sideslip angles over 2 degrees [Liebemann *et al.*, 2005].

Another important state to keep track on is the roll angle, that is the angle between the inertial *xy*-plane and the vehicle's *xy*-plane. A large roll angle increases the risk that the bus exhibits a rollover, something that mostly occurs on high friction road since then the lateral forces may be large.

With the above discussion in mind, the plots for the vehicle states will contain the longitudinal velocity, the yaw rate, the sideslip angle, the limit of the maximum allowed sideslip angle given by (6.1) and the articulation angle. The roll angle is also considered, but it is not shown in the plots because the primarily goal of the ESP is to control the yaw rate and the sideslip angle. If those two states are controlled in a proper way, the risk of rollover is greatly decreased. This is because many rollover accidents occur when the vehicle is skidding and encounters a high friction road. Note that only the states for the tractor are shown because the ESP will control the yaw rate of the front part, leading to indirect control of the trailer as well.

6.2 Test Maneuvers

All maneuvers were tested on different surfaces, with different velocities. The range of friction values used were $0.2 \leq \mu \leq 1.2$, which roughly corresponds to a range from icy road to dry asphalt. The velocities tested spanned from about 10 m/s to 30 m/s, which should cover a lot of different conditions. Two of the maneuvers that were used on the bus are listed and explained below. Other maneuvers were, of course, tested as well, but priority were given to the following two since they are standard maneuvers, intended for the investigation of vehicle stability.

Fishhook

The fishhook maneuver is a very common maneuver to test yaw and roll stability of vehicles. It can be considered to emulate a situation where collision avoidance is desired. The maneuver, which was originally defined by Toyota, is carried out as follows[1] [Schindler, 2007]:

- The steering wheel is increased at a rate of 700 deg/s until the limit $6.5\delta_s$ is reached, where δ_s is the steering wheel angle that is required to reach a stationary lateral acceleration of $0.3g$ m/s^2 on a dry road.
- The value obtained is held for 250 ms.
- The steering wheel is turned the opposite way with the same speed until it reaches -$6.5\delta_s$.
- After 3 seconds the steering wheel is turned back to 0 degrees.

The maneuver can be seen in Figure 6.1.

[1] With some slight modifications depending on the type of vehicle.

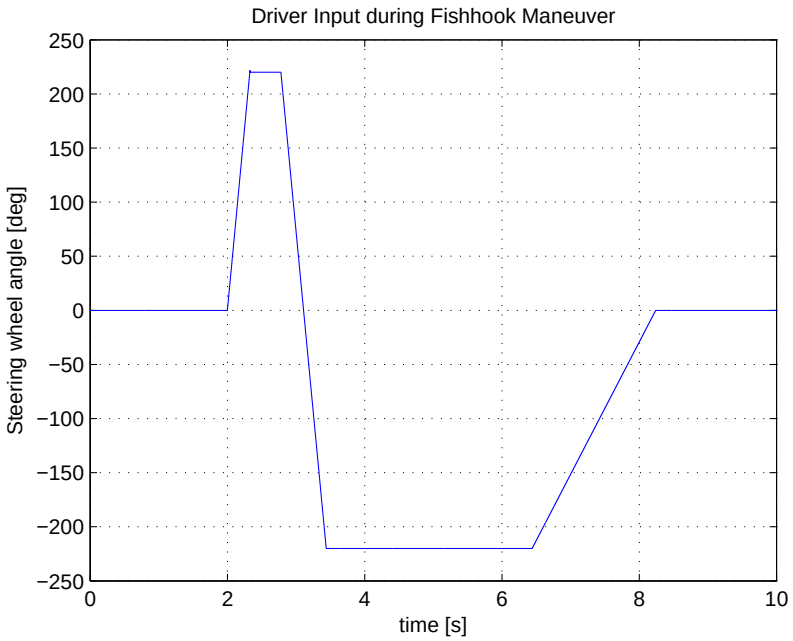

Figure 6.1 Driver input during the fishhook maneuver. This maneuver is very common when it comes to determine yaw and roll stability of vehicles.

J-Turn

This maneuver is a standardized test maneuver by the NHTSA. The maneuver is started by turning the steering wheel at 900 deg/s until a value of $8\delta_s$ is reached, and is shown graphically in Figure 6.2.

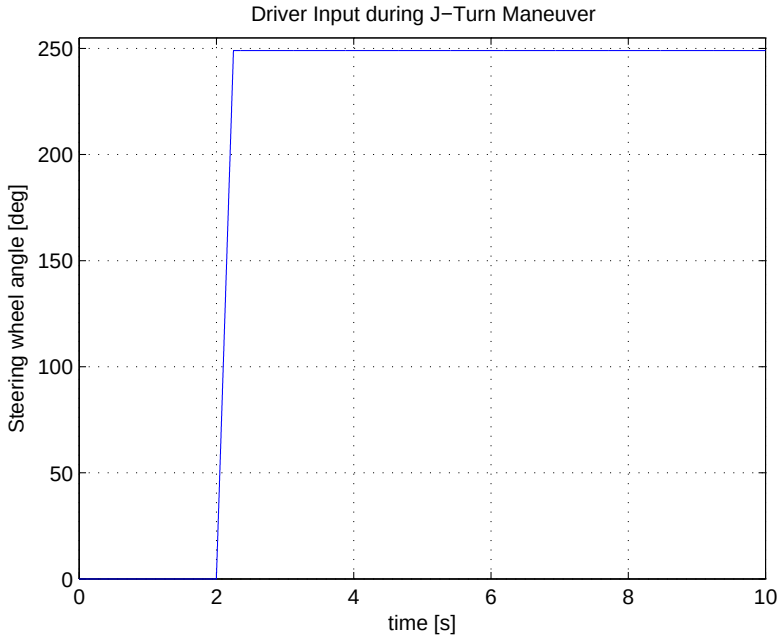

Figure 6.2 Driver input during the J-turn maneuver.

6.3 Simulation Results

The controller parameters are shown in Table 6.1. It should be noted that the moment of inertia I_{zz1} used in the controller is that of the fully loaded bus.

The figures will show some relevant vehicle states, the reference slip for the wheels and also the brake pressures. In the plots for the vehicle sideslip angle β, the maximum allowed sideslip angle earlier defined as

$$\beta_{max} = 10 - 7\frac{v^2}{40^2}$$

is dashed, and in the plots for the yaw rate the actual yaw rate and reference are denoted 'measured' and 'Reference', respectively.

Table 6.1 Controller parameters used in the simulations. Several different configurations worked well.

Controller gain	η	1.5
Saturation factor	ε	0.08
Distribution factor	k_s	0.7

J-Turn Maneuver

The loading conditions are those of a fully loaded bus and the friction coefficient is set to $\mu = 1$.

Controller Inactive Some important vehicle states are shown in Figure 6.3 for the J-turn maneuver with the ESP turned off. As can be seen from the plots, the bus is unstable. The side slip angle grows fast, and the articulation angle reaches over 90 degrees within 4 seconds from the maneuver start. In fact, the vehicle stops after approximately 6 seconds because of the skidding.

Controller Active The vehicle states are stable when the controller is active. From Figure 6.4 one can see that β is well below the maximum. The articulation angle is also stabilized.

When looking at the yaw rate plot one has to take into consideration that the ESP does not try to track the reference exactly, since in the design in Chapter 6 a threshold for when the ESP should intervene was set. With this in mind the tracking can be considered good.

In Figure 6.5 the slip values, denoted 'Actual', for each of the wheels are shown. From the plots it is possible to come to the conclusion that the signum function approximated as a saturation in Chapter 6 makes the control rather smooth, while still keeping the stability intact. The slip follows its reference in a good manner, ensuring that the desired moment will be produced.

The brake pressures corresponding to the slip values are depicted in Figure 6.6. One can notice the difference in brake inputs between the front right and middle left wheel although they have about the same slip. The reason for this is the load transfer of the bus, which puts a greater load on the right wheels than those on the left for this maneuver. It is also because of this the brake pressure is exhibiting a large overshoot for the middle left wheel: the load on this wheel is almost zero.

Trajectories The trajectories for the controlled and uncontrolled bus are shown in Figure 6.7. It is clear from this plot that the radius of curvature for the bus when the ESP is active is much smaller than in the uncontrolled case. This may be of interest since the reason for performing a J-turn or fishhook maneuver can be to try to reach a missed exit on a road, or even collision avoidance. In these cases it is important that the ESP is not too restrictive. One can note that the yaw rate of the uncontrolled bus is higher than in the controlled case, which could imply that the radius of curvature should be smaller. The reason for why this is not the case is that the bus is spinning.

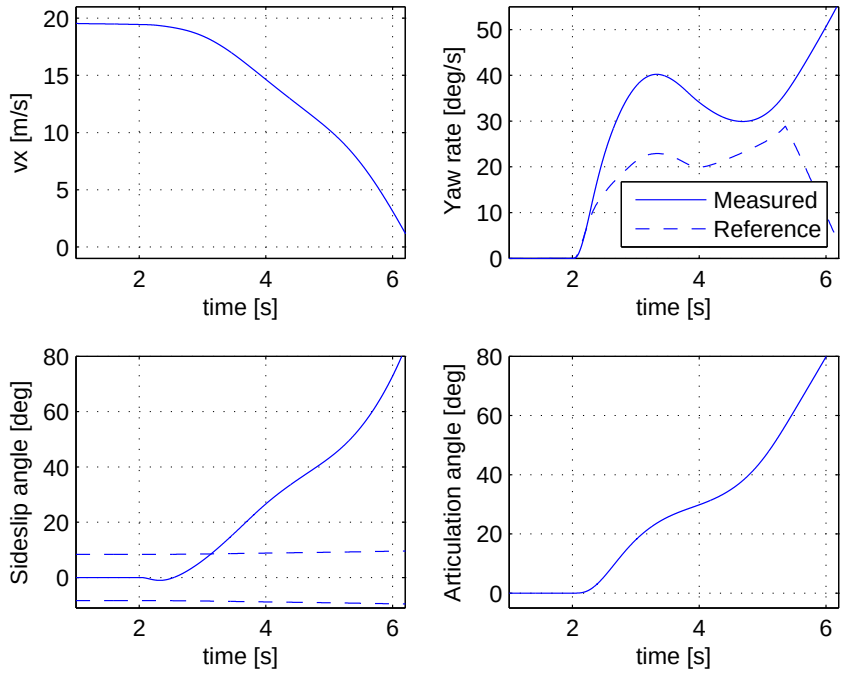

Figure 6.3 The vehicle states for the J-turn maneuver with the ESP inactive and with an entrance speed of approximately 70 m/s. The bus is fully loaded. The instability is clear from the plots.

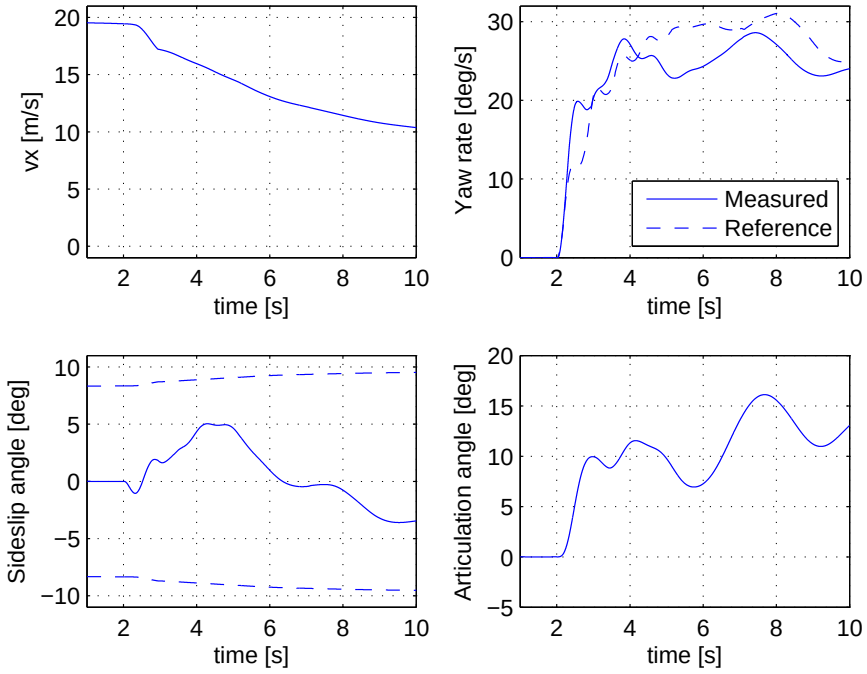

Figure 6.4 The vehicle states for the J-turn maneuver with the ESP active and with an entrance speed of approximately 70 m/s. Now the states are stable due to the good yaw rate tracking.

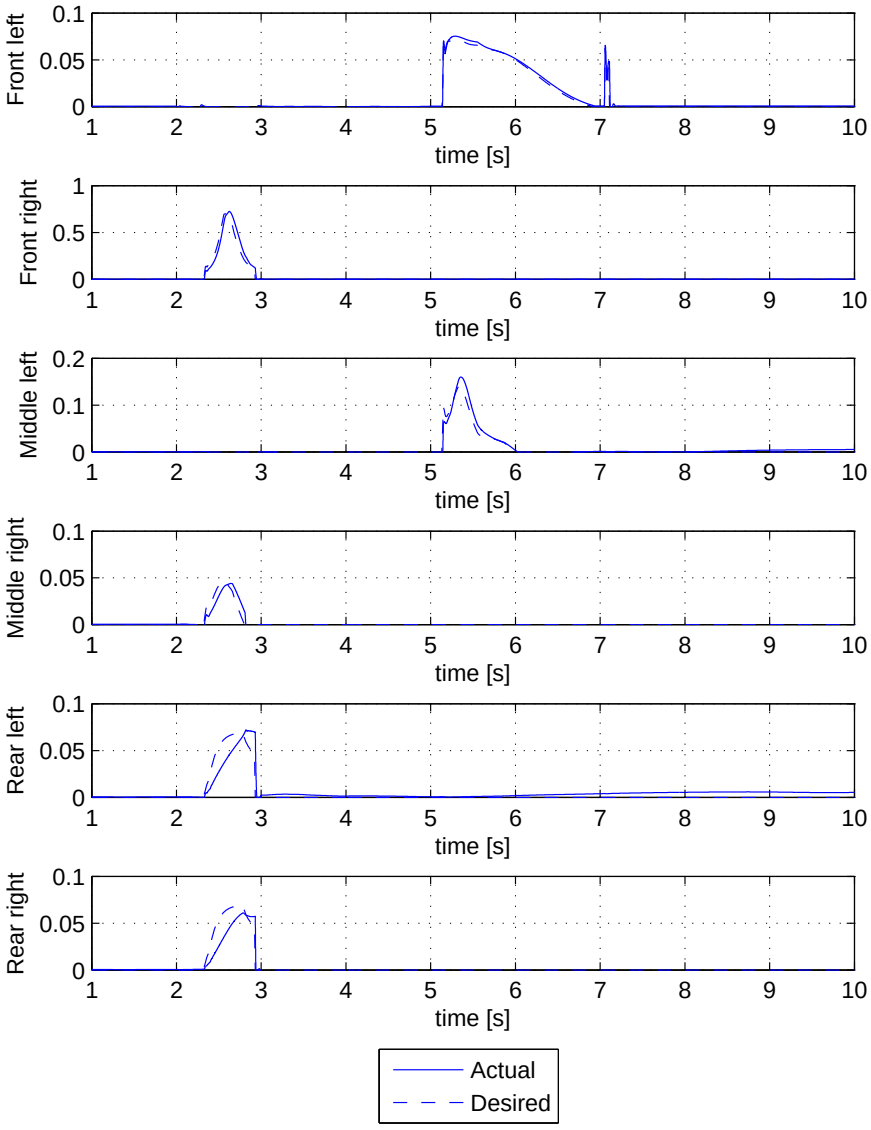

Figure 6.5 The slip value for each wheel together with desired slip, marked as dashed in the plot, during J-turn maneuver for the fully loaded bus.

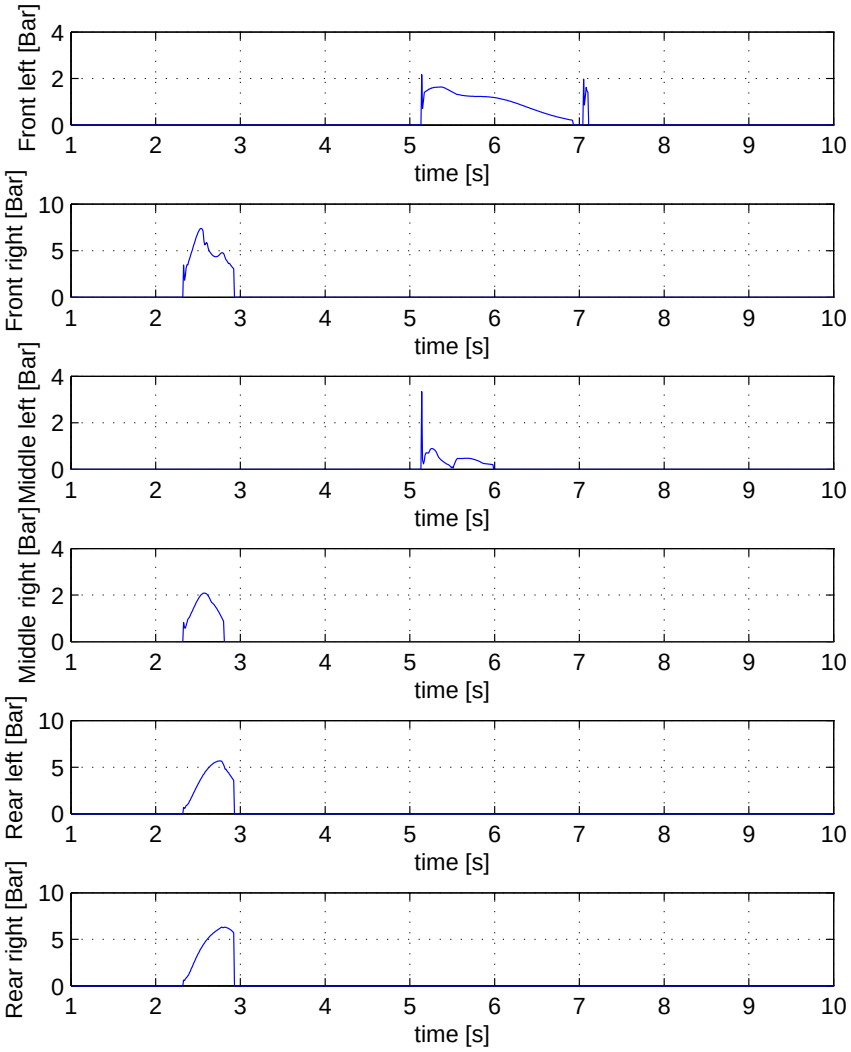

Figure 6.6 The brake pressures during the J-turn maneuver corresponding to the slip values in Figure 6.5. Note the overshoot for the third wheel due to load transfer.

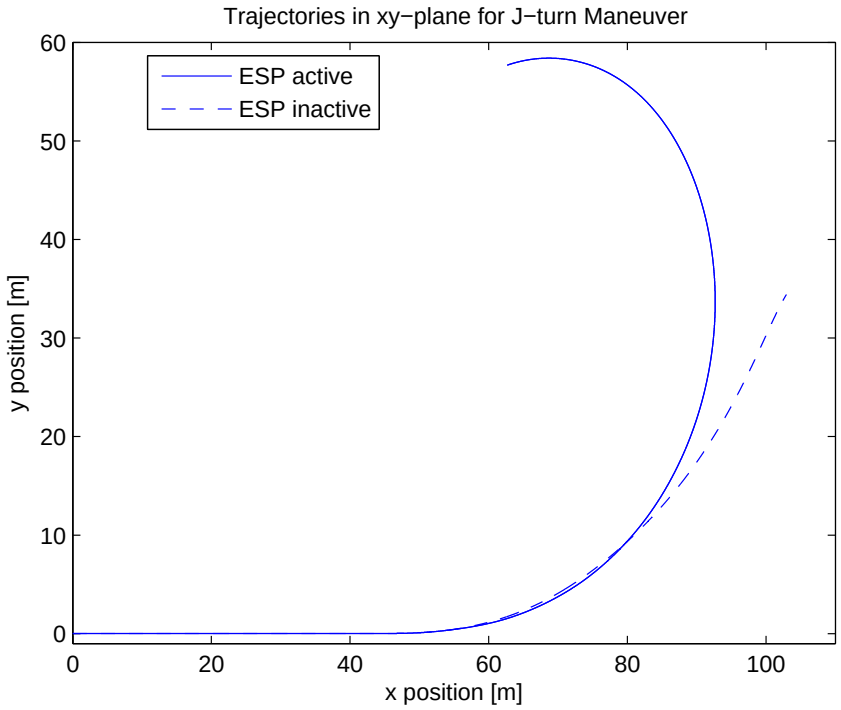

Figure 6.7 Bus trajectories for the J-turn maneuver. The trajectories of the uncontrolled bus is marked as dashed. The improvement in curvature handling with the ESP active is rather significant, which is a sign of that the yaw rate reference is not too restrictive.

Fishhook Maneuver for the Loaded Bus

The results of the fishhook maneuver in this section is for the case when the bus is fully loaded. The friction coefficient $\mu = 1$.

Controller Inactive In Figure 6.8 the simulation results for the fully loaded bus when the ESP is inactive are illustrated. The sideslip angle is above the limit already after 1 second into the maneuver, and the yaw rate shows a really unstable behaviour with the limit exceeded by more than a factor 2. The articulation angle peaks at 80 degrees, before the bus eventually stops due to spin-out.

Controller Active From Figure 6.9 it is noticeable that the bus now remains stable. The tracking of the yaw rate is very good, and the sideslip angle is way below the limit. The articulation angle is also kept stable, preventing jackknifing, although the oscillations are quite significant. This is partly due to the high entrance speed, but also because this maneuver really shows the dynamics of the bus.

The reference slip can from Figure 6.10 be seen to reach its limit. This means that an increase in the controller gain will not lead to much change in the behavior for this maneuver. The limits for maximum reference slip can be modified to reach the desired yaw rate faster for the oversteering at 4 seconds. However, increasing the limit for the front outer wheel will make the risk of wheel lock larger, something which is highly undesired. In any case, the slip is following its reference very quickly. The corresponding brake pressures are visible in Figure 6.11. This shows that the ABS is rapid and fulfills its goal even during extreme cornering: to control the slip.

Trajectories The trajectories for the fishhook maneuver are depicted in Figure 6.12. The same conclusions can be drawn here as before, namely that with the ESP active the bus performs better.

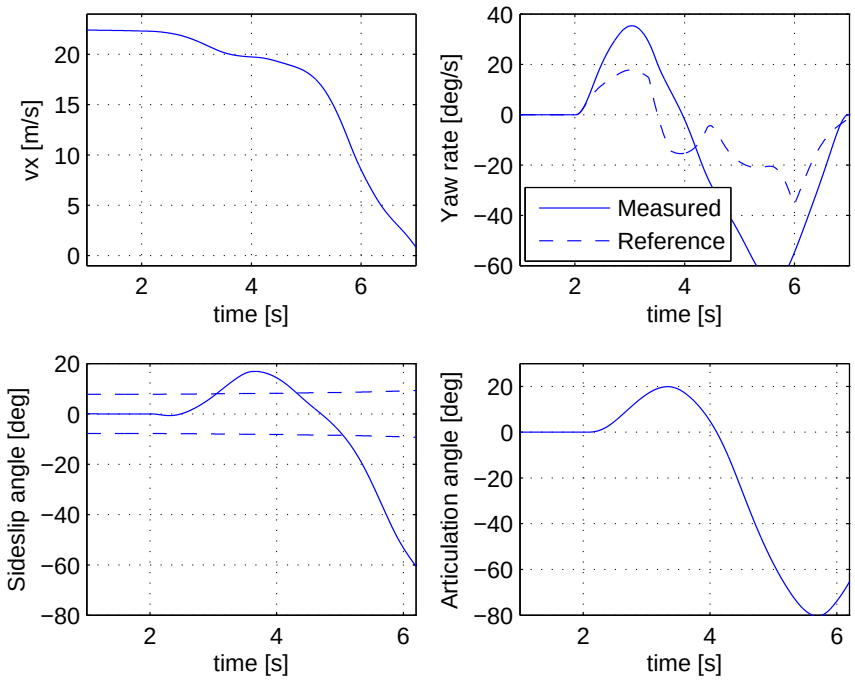

Figure 6.8 The vehicle states for the fishhook maneuver with the ESP inactive and an entrance speed of 83 km/h. The bus is fully loaded. The severe instability is clearly visible.

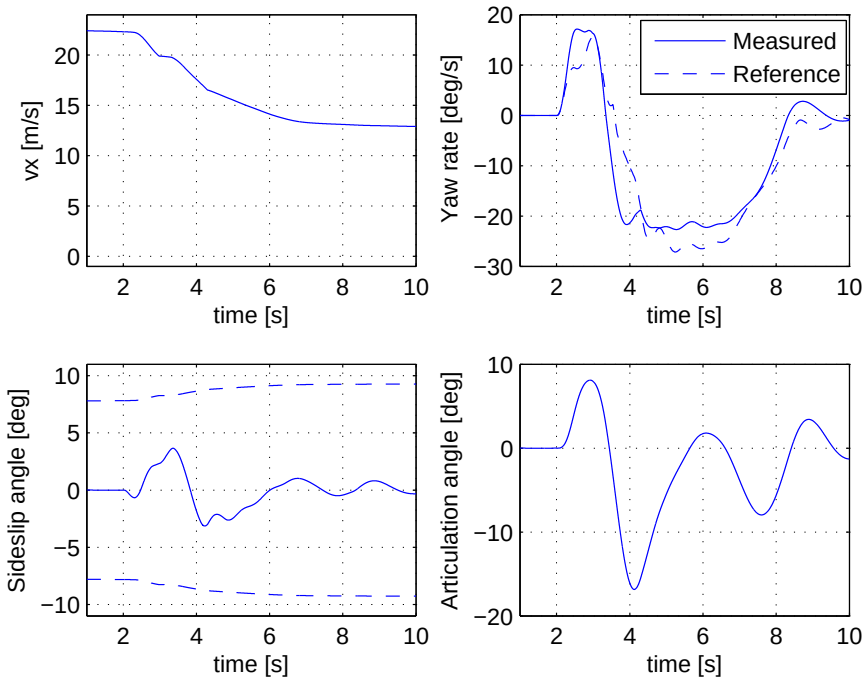

Figure 6.9 The vehicle states for the fishhook maneuver with the ESP active and an entrance speed of 83 km/h. The bus is now stable and the improvement by using ESP compared to Figure 6.8 is obvious. The bus is fully loaded.

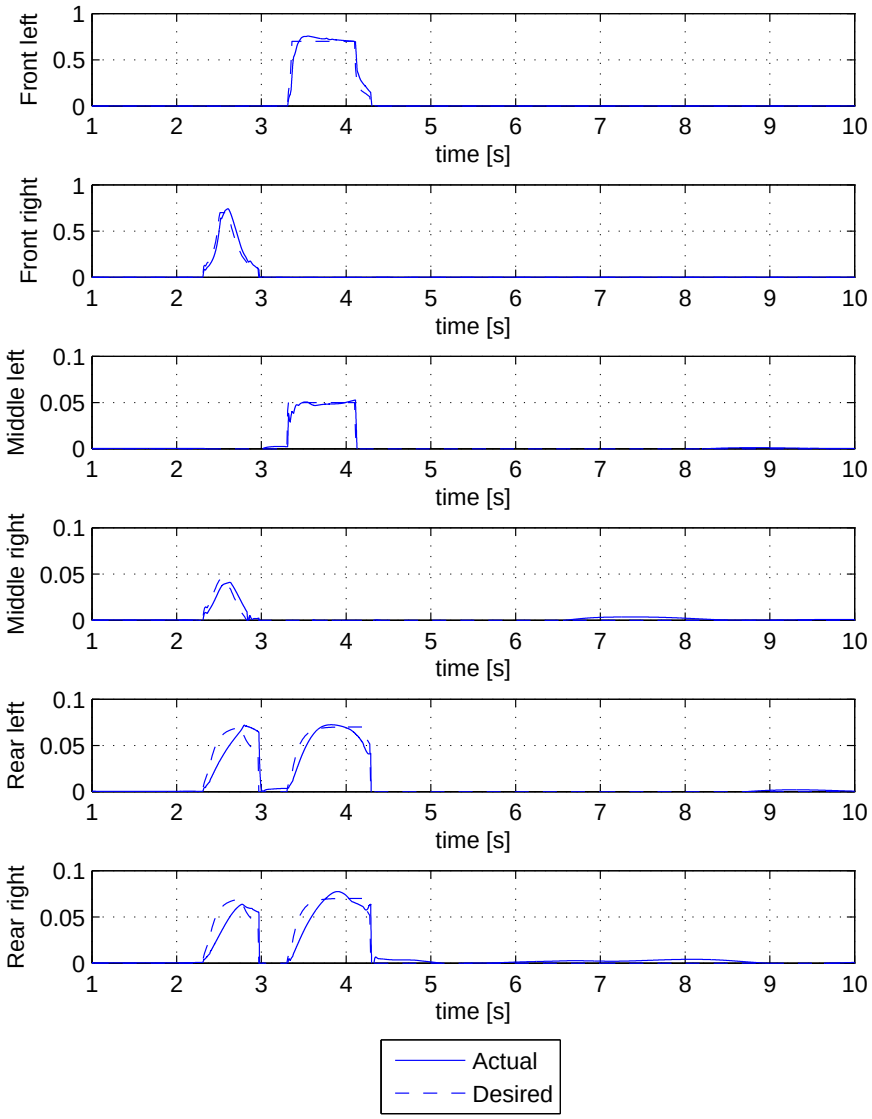

Figure 6.10 The longitudinal slip values together with the desired slip during the Fishhook maneuver and with the bus fully loaded. The reference is followed very satisfactory. Note the short amount of time the ESP is active, enough to completely change the behavior of the bus.

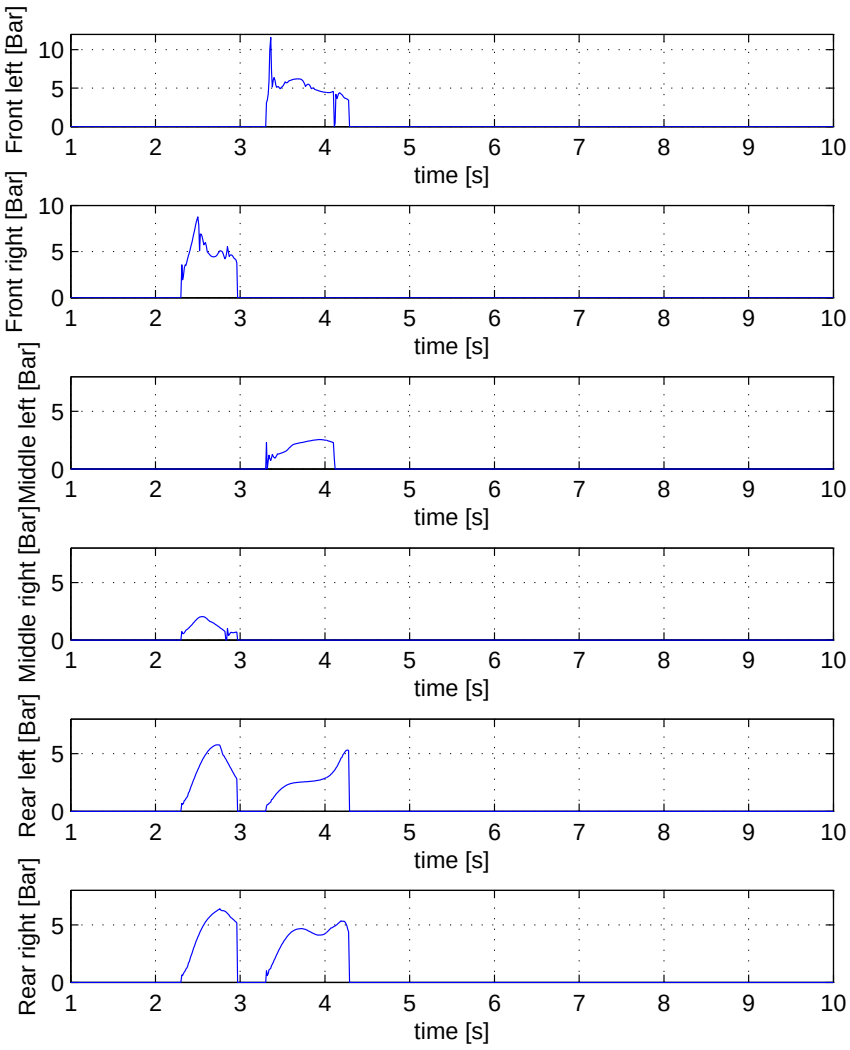

Figure 6.11 The brake pressures for the wheels during the Fishhook maneuver when the bus is fully loaded. Note the quick reaction in brake pressure for the front wheel. This ensures fast tracking of the reference slip.

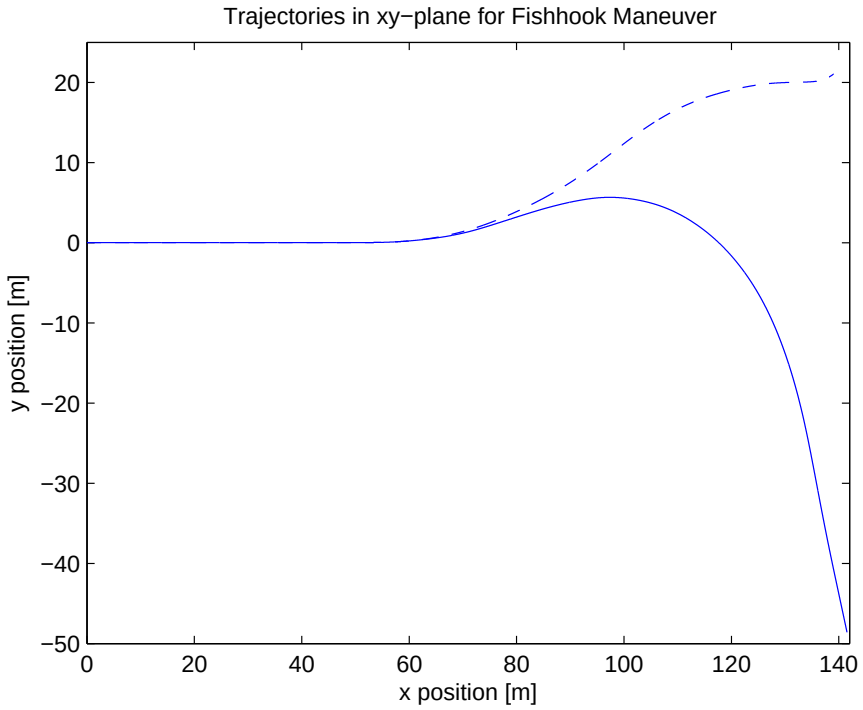

Figure 6.12 Bus trajectories for the Fishhook maneuver when the bus is fully loaded. The ESP, despite that it limits the yaw rate, increases the performance of the bus in terms of corner handling.

Fishhook Maneuver for Semi-Loaded Bus

The results so far have proved that the ESP is capable of stabilizing some extreme maneuvers at high speed. For a situation where the ESP is not capable of stabilizing the bus completely, a simulation where the first part of the bus is loaded and the second is empty will be given. The uncontrolled bus is of course unstable and the plots are left out for this case. The friction coefficient is set to 0.5, corresponding to a very wet road.

The plots for the controlled case are provided in Figure 6.13. In this case the ESP is unable to stabilize the bus, which is because of two reasons: First of all, the trailer starts to skid early in the maneuver with a large articulation angle as a result which drags the tractor with it. The second reason is that the low friction coefficient unables the necessary moments to be produced to keep the bus stable. This can also be observed from Figure 6.14, where the reference slip values reach their allowed limit. At first it seems like the necessary moments may be produced if the desired slip values are not saturated at all and by increasing the controller gain. This was also tried out, with $\eta = 3$, which yielded better tracking of the yaw rate, but still not enough to follow the reference at the end of the simulation.

The brake pressures in Figure 6.15 further verifies the fast response of the ABS.

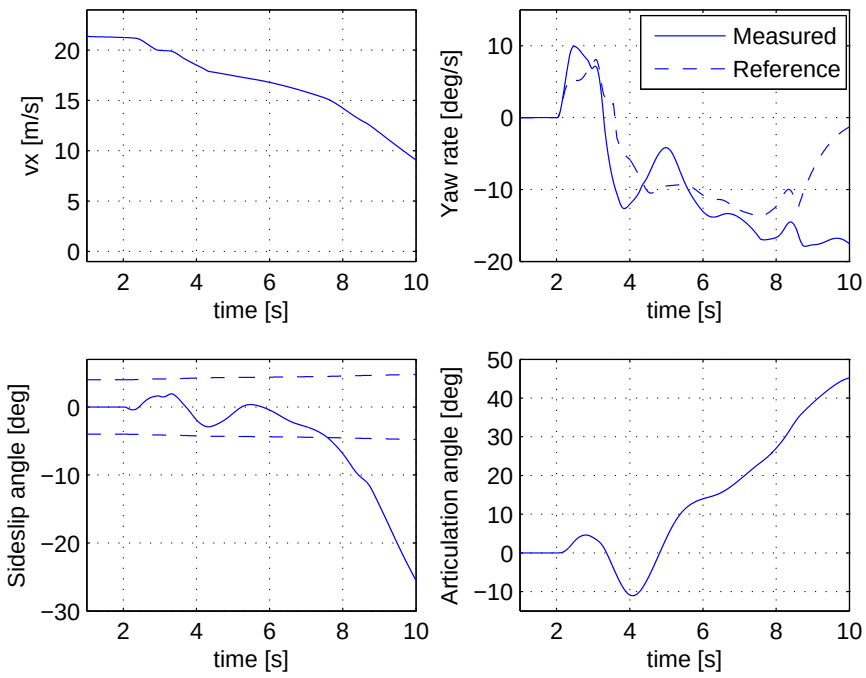

Figure 6.13 Vehicle states for the fishhook maneuver with the semi-loaded bus and with the fricion coefficient $\mu = 0.5$. The ESP is not able to stabilise the bus during the whole maneuver.

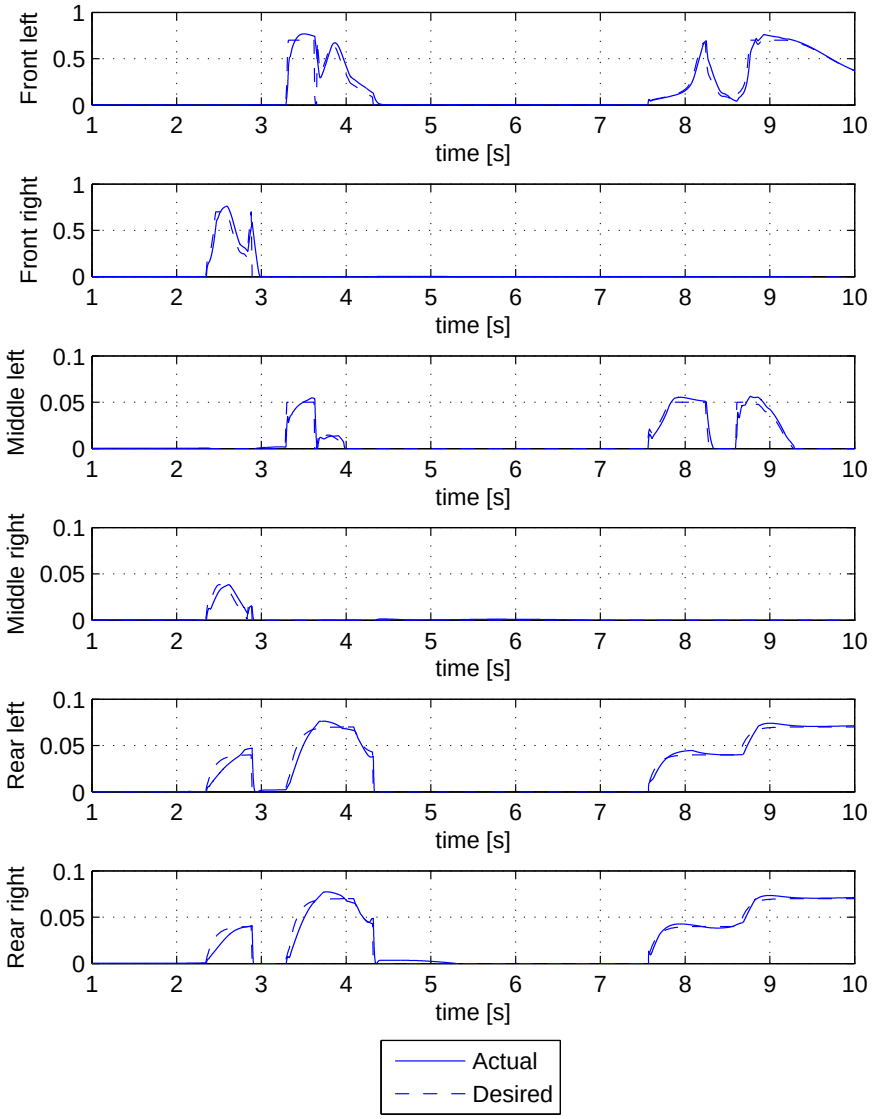

Figure 6.14 The slip values together with the desired slip during the fishhook maneuver with the first part of the bus fully loaded and the friction coefficient set to 0.5. The slip values follow its reference smoothly.

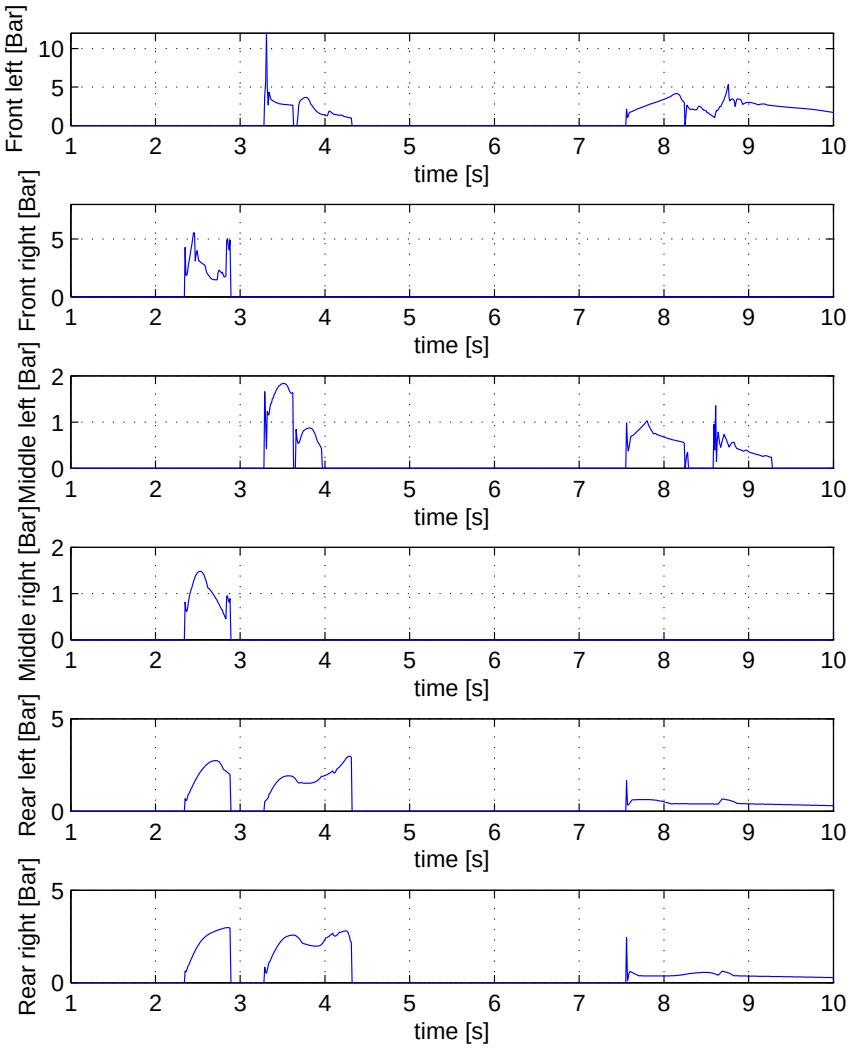

Figure 6.15 The brake pressures during the fishhook maneuver with the first part of the bus fully loaded and the friction coefficient set to 0.5.

6.4 Discussion

In this section the performance of the controller is discussed and some conclusions are drawn.

Yaw Rate Controller

The performance of the yaw rate controller was found to be good. The reference tracking works well for different loading conditions, showing the robustness of the controller to parameter uncertainties. Despite the high-gain properties of the controller, the tracking of the yaw rate can be seen to be rather smooth. For the simulations when the yaw rate could not be followed it was not because of the controller used, but rather because the forces between the wheels and the road were not large enough to produce the desired yaw rate. For a heavy articulated vehicle, the problem of having the wheels producing necessary moments are more emphasized than for regular cars. This is because of the large moments these type of vehicles have.

The thresholds used for when the controller is active may be tweaked somewhat for better performance, but this will probably not have any major impact on the performance. The controller is active a short amount of time during the maneuvers, while still maintaining stability in most cases.

Yaw Rate Reference Model

The linear one-track model, together with the limiting of the yaw rate via the actual lateral acceleration, has been proved to work well in terms of stabilization of the bus. There are also other possibilities that could have been tried out, for example by limiting the input to the model by knowing the maximum lateral friction coefficient and the steady state relation between steering angle and lateral acceleration, for example taken from a simplified one-track model. Better friction modeling than the one used in this thesis is, however, needed in order for that to work well, something which is not likely to be available in a commercial bus.

Slip Generation Performance

The generation of the desired slip through the use of the Kamm-circle model, together with the load transfer model, performed well throughout the tests. Simulations, for this bus and also for a regular car in [Kiencke and Nielsen, 2005], have shown that the load transfer model is accurate in predicting the change of load due to cornering. As discussed before the limitation of the reference could have been set less conservatively, but that only produces small positive changes in control performance at the cost of the risk of wheel lock. Clear from the plots is that the slip follows the reference in a smooth and fast fashion. This is important since the achievable yaw rate control performance greatly depends on that the desired moment can be produced fast.

Conclusions

The simulations show that the ESP performs very well, although there are some unpleasant results that need to be considered: First of all, there is the problem that the articulation angle is oscillating, and for some maneuvers the oscillations are quite severe. The ESP prevents the bus from jackknifing, but it would be convenient to get rid of the oscillations. Secondly, the ESP can not always keep the bus stable. This happens mostly at low friction coefficients where the forces that are possible to generate are smaller than on high friction. These problems were noticed for other types of maneuvers as well, but seldom with the severe instablity shown here. Although the maneuvers and velocities used for the simulations are rather extreme, it

still shows that there is room for improvement. Therefore the conclusion is drawn that even though the ESP performs very well and is able to stabilize the bus and prevent jackknifing in most driving conditions, the stability of the bus is still endangered at some combinations of speed, friction coefficient and maneuver.

6.5 Stabilization at Low Velocities

There are situations when jackknifing is a concern even at low velocities, some of which have been investigated in this work. As an example, when driving out from a busstop on slippery or snowy roads the risk of jackknifing is quite significant.

Control Strategy

Consider Figure 6.16 where the driver is turning while accelerating, with the resulting accelerating torque denoted M_A. If a brake pressure is added to the left wheel, corresponding to a braking torque M_B, the result will be a positive moment about the center of gravity and thus $\Delta\psi$ will decrease. In order to have the same acceleration before and after the brake pressure is added, the following must hold:

$$M_A = -M_B + M_A^*,$$

where M_A^* is the accelerating torque needed to have the same resulting acceleration despite a brake input. Note that the result of accelerating even more will further decrease $\Delta\psi$ because of an added torque coming from the right wheel[2].

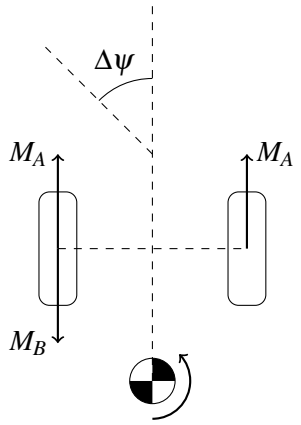

Figure 6.16 By braking the left wheel the articulation angle will decrease. In order to have the same acceleration, the accelerating moment has to be increased.

ESP Inactive Consider Figure 6.17 where the vehicle states for a 160 degrees step input are depicted. The friction coefficient is set to $\mu = 0.4$, and the ESP is inactive. The bus jackknifes and starts to spin after a couple of seconds.

ESP Active In order to control the articulation angle, it is preferable to know the articulation angle as a function of velocity and steering wheel angle. For this purpose a linear steady state dependence was estimated by doing some step inputs of different magnitude at different velocities.

[2] M_B and M_A are larger than or equal to zero.

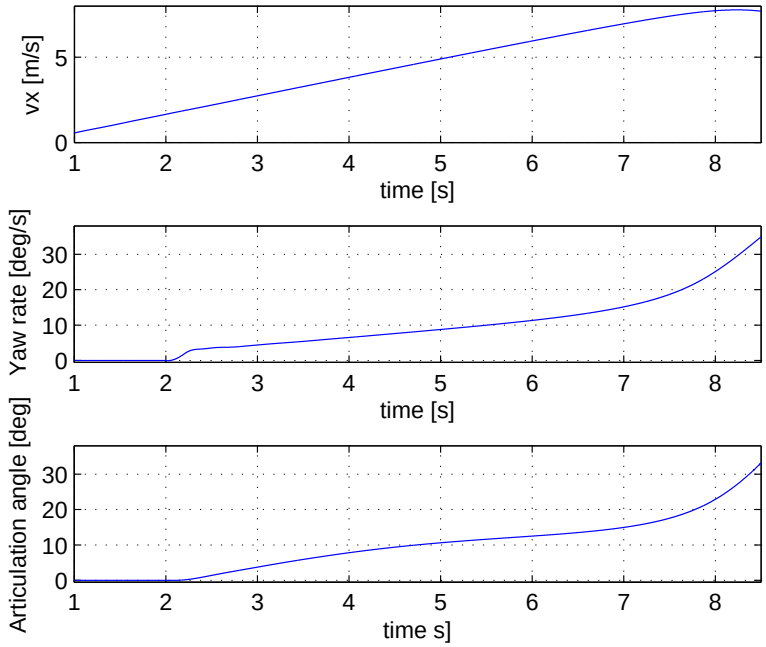

Figure 6.17 A 160 degrees step input is activated at 2 seconds. The ESP is inactive.

The following figure, Figure 6.18, shows the states when the ESP is activated. The ESP intervenes by feeding the ASR with a reference slip of -1% when the articulation is larger than the linear steady state dependence, marked as dashed in the lower plot. It is possible to see that the states are stable, but oscillations appear in both yaw rate and articulation angle. When inspecting Figure 6.18 it is worthwhile to remember that the ESP does not intervene continously. If a more advanced reference model is derived, so that it is possible to intervene earlier, the oscillations can hopefully be removed.

Discussion

This section was aimed at investigating whether the ESP can be used to stabilize the bus at low speed. Indeed, the simulations show that the ESP stabilizes the bus for the considered maneuver. It is likely that the oscillations in the articulation angle can be removed by using a more advanced strategy in terms of reference generation and intervention.

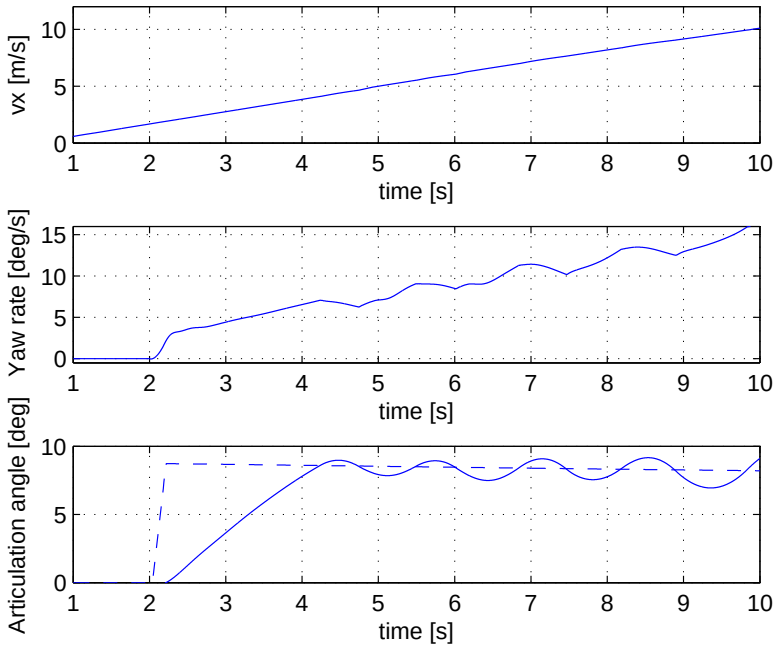

Figure 6.18 A 160 degrees step input with $\mu = 0.4$ and the ESP active. It is seen, when comparing to Figure 6.17, that the bus is stabilized.

7. Conclusions and Future Work

7.1 Conclusions

The main focus of this work has been on designing and implementing an ESP in Simulink. The ESP is split up into two parts, where one part deals with calculating a stabilizing moment about the center of gravity of the tractor and the other part maps this moment to the wheels via the ABS and the ASR. Simulation results have shown both that the ESP alone is capable of stabilizing some extreme maneuvers at high speed and that it is robust to various loading conditions. However, yaw rate and sideslip angle stability can not always be guaranteed, the main reason being the oscillations of the trailer. The ESP has first and foremost been designed to stabilize the yaw rate, which hopefully implies that the sideslip angle and articulation angle are also stabilized. From Chapter 6 it should be clear that this strategy is succesful, where the articulation angle is stable if the yaw rate is stable. The strategy to brake both trailer wheels have proved to work well, but it is still possible that other strategies may give better performance.

7.2 Future Work

Reference Model

Many different maneuvers have been performed to verify the tractor one-track model for reference generation. Tests carried out so far have shown that the model does not trigger the ESP more than necessary, although further investigation needs to be undertaken. If the model is found to be obsolete several solutions exists, as discussed in Chapter 6. One solution is to losen the thresholds for when to intervene. Another possibility is to use the more advanced linear model derived in Section 2.5.

Closed-Loop Driving

The driving situations were performed in open-loop, which means that predefined input maneuvers have been used. To instead have a closed-loop driver model may give more realistic situations. It is conceivable that the driver behaves differently than in the open-loop maneuvers; the driver may for example start to brake when in a critical situation, which may cause problems for the controller.

Tests in a Real Bus

As mentioned several times, the simulator used is highly realistic. Still, tests in a real bus are important since a real environment introduces several uncertainties that may alter the performance of the ESP, for example noise in measurements, additional delays and dynamics.

8. Bibliography

Burton, D., A. Delaney, S. Newstead, D. Logan, and B. Fildes (2004): "Evaluation of Anti-lock Braking Systems Effectiveness." Research Report No. 04/01. Royal Automobile Club of Victoria Ltd.

Eisele, D. and H. Peng (2000): "Vehicle Dynamics Control with Rollover Prevention for Articulated Heavy Trucks." *5th International Symposium on Advanced Vehicle Control, Michigan.*

Fontes, M. (2007): "Lecture Notes in Mathematical Structures." Lund Institute of Technology, Sweden.

Gäfvert, M., M. Sanfridson, and V. Claesson (2000): "Truck Model for Yaw Dynamics Control." Technical Report ISRN LUTFD2/TFRT--7588--SE. Department of Automatic Control, Lund Institute of Technology, Sweden.

Glad, T. and L. Ljung (2003): *Reglerteori- Flervariabla och olinjära metoder*, second edition. Studentlitteratur.

Isermann, R. (2006): *Fahrdynamik-Regelung*. Vieweg Verlag.

Khalil, H. K. (2000): *Nonlinear Systems*, third edition. Prentice Hall.

Kiencke, U. and L. Nielsen (2005): *Automotive Control Systems- For Engine, Driveline and Vehicle*, second edition. Springer.

Klĕcka, R. (2007): "Vehicle Model for Dynamics Analysis and HIL Simulation." Technical Report. Department of Control Systems and Instrumentation, Faculty of Mechanical Engineering, Technical University of Ostrava.

Lie, A., C. Tingvall, M. Krafft, and A. Kullgren (2005): "The effectiveness of Electronic Stability Control in reducing real life crashes and injuries." *19th International Conference on the Enhanced Safety of Vehicles Conference (ESV) 2005*, **No 05-0135**.

Liebemann, K., K. Meder, J. Schuh, and G. Nenninger (2005): "Safety and Performance Enhancement: The Bosch Electronic Stability Control." Paper Number 05-0471. Robert Bosch GmbH.

Petersen, I. (2003): *Wheel Slip Control in ABS Brakes using Gain Scheduled Optimal Control with Constraints*. PhD Thesis ISBN 82-471-5593-1, Department of Engineering Cybernetics, Norwegian University of Science and Technology, Trondheim, Norway.

Rajamani, R. (2006): *Vehicle Dynamics and Control*. Springer US.

Schindler, E. (2007): *Fahrdynamik: Grundlagen Des Lenkverhaltens Und Ihre Anwendung Für Fahrzeugregelsysteme*. Expert-Verlag.

Schofield, B. (2008): *Model-Based Vehicle Dynamics Control for Active Safety*. PhD Thesis ISRN LUTFD2/TFRT--1083--SE, Department of Automatic Control, Lund University, Sweden.

Solyom, S. (2002): *Synthesis of a Model-based Tire Slip Controller*. Licentiate Thesis ISRN LUTFD2/TFRT--3228--SE, Department of Automatic Control, Lund Institute of Technology, Sweden.

Åström, K. J. and R. Murray (2008): *Feedback Systems: An Introduction for Scientists and Engineers*. Princeton University Press.

Åström, K. J. and B. Wittenmark (1997): *Computer Controlled Systems: Theory and Design*, third edition. Prentice Hall.

Svendenius, J. (2007): *Tire Modeling and Friction Estimation*. PhD Thesis ISRN LUTFD2/TFRT--1077--SE, Department of Automatic Control, Lund University, Sweden.

Tøndel, P. and T. A. Johansen (2005): "Control Allocation for Yaw Stabilization in Automotive Vehicles using Multiparametric Nonlinear Programming." Technical Report. Department of Engineering Cybernetics, Norwegian University of Science and Technology, Trondheim, Norway.

A. Nomenclature and Definitions

A.1 Abbreviations

Below are the abbreviations used in the thesis.

ESP	Electronic Stability Program(s)
ABS	Anti-lock Braking System
ASR	Anti-Spin Regulation
CoG	Center of Gravity
NHTSA	National Highway Traffic Safety Administration
PID	Proportional-Integral-Derivative
CASCaDE	Computer Aided Simulation of Car, Driver and Environment

A.2 Symbol Descriptions

The table below summarizes the most frequently used symbols used in the thesis. Some of the symbols may have an additional index referring to for example front or rear part of the bus; that is not included here.

Symbol	Description
x	Longitudinal position in a certain frame
y	Lateral position in a certain frame
z	Vertical position in a certain frame
g	Gravitational constant
Vehicle variables	
v_x	Longitudinal velocity
v_y	Lateral velocity
a_y	Lateral acceleration
δ	Steering angle (at the wheels)
δ_s	Steering angle used in fishhook and J-turn
$\Delta\psi$	Articulation angle
$\dot{\psi}$	Yaw rate
β	Sideslip angle as defined in (2.4)
F_{xp}	Longitudinal contact point force
F_{yp}	Lateral contact point force
F_f	Vertical static front axle force

F_m	Vertical static middle axle force
F_r	Vertical static rear axle force
F_p	Vertical static contact point force
ΔF_{xf}	Longitudinal load transfer at front axle
ΔF_{xm}	Longitudinal load transfer at middle axle
ΔF_{xr}	Longitudinal load transfer at rear axle
ΔF_{xp}	Longitudinal load transfer at contact point
ΔF_{yf}	Lateral load transfer at front axle
ΔF_{ym}	Lateral load transfer at middle axle

Vehicle parameters

m_1 (m_2)	Mass of front (rear) part
l_f	Distance between tractor *CoG* and front axle
l_m	Distance between tractor *CoG* and middle axle
l_r	Distance between trailer *CoG* and rear axle
x_1	Distance between front axle and contact point
x_2	Distance between tractor *CoG* and contact point
x_3	Distance between middle axle and contact point
x_4	Distance between trailer *CoG* and contact point
x_5	Distance between rear axle and contact point
l_m^*	Extension factor in one-track model
y_f	Half track width of front axle
y_m	Half track width of middle axle
y_r	Half track width of rear axle
I_{zz}	Moment of inertia about *CoG* z-axis
I_1 (I_2)	Moment of inertia about contact point z-axis

Tire variables

α	Wheel tire slip angle as defined in (2.3)
α_f (α_m) (α_r)	Tire slip angle of 1st (2nd) (3rd) wheel in one-track model
λ	Longitudinal slip as defined in (2.1) and (2.2)
ω	Wheel rotational velocity
v_{wx}	Wheel longitudinal velocity
v_{wy}	Wheel lateral velocity
F_x	Longitudinal tire force
F_y	Lateral tire force
F_z	Vertical tire force
μ	Maximal friction coefficient between tire and road
P_B	Brake pressure
M_B	Brake torque
M_A	Drive torque

Tire parameters

C_α	Cornering stiffness
C_λ	Longitudinal stiffness
I_w	Moment of inertia
m^*	Mass resting on the wheel
r	Effective wheel radius
C_B	Proportional factor between M_B and P_B

Control symbols

K	ABS and ASR proportional gain
T_i	ABS and ASR integral gain
T_d	ABS and ASR derivative gain
e_λ	Longitudinal slip control error
C_{ABS}	Transfer function between P_B and e_λ
η	Yaw rate control gain
ε	Yaw rate control smoothing factor
k_s	Distribution factor for M_{yaw}
J	Time constant for switching strategy
T_s	Sampling time
M_{yaw}	Yaw rate control moment

A.3 Mathematical Definitions

In this section various mathematical definitions are placed that did not fit into the text. The definitions are taken from [Fontes, 2007].

Continuity of Functions

DEFINITION A.1
Let $x \in \mathbf{R}^n$. A function $f : \mathbf{R}^n \to \mathbf{R}^p$ is continous at a point $a \in \mathbf{R}^n$ if and only if for any $\varepsilon > 0$ there exists a $\delta > 0$ such that

$$||f(x) - f(a)|| < \varepsilon \text{ if } ||x - a|| < \delta$$

The function is said to be continous if it is continous at all points in $\mathbf{R}^n$ □

DEFINITION A.2
Let $x \in \mathbf{R}^n$. A function $f : \mathbf{R}^n \to \mathbf{R}^p$ is uniformly continous if and only if for any $\varepsilon > 0$ there exists a $\delta > 0$ such that

$$||f(x) - f(a)|| < \varepsilon \text{ if } ||x - a|| < \delta$$

for all $a \in \mathbf{R}^n$

□

DEFINITION A.3
A function $f : \mathbf{R}^n \rightarrow \mathbf{R}^p$ is Lipschitz continous, with Lipschits constant L, if and only if there exists a constant $L > 0$ such that

$$||f(x) - f(a)|| \leq L||x - a|| \; ; x, a \in \mathbf{R}^n$$

□

B. Additional Plots

B.1 ABS Plots

Below are listed the resulting slip for the ABS for the first and fifth wheel as well, to show the results for all axles.

Emergency Braking for $\mu = 1$

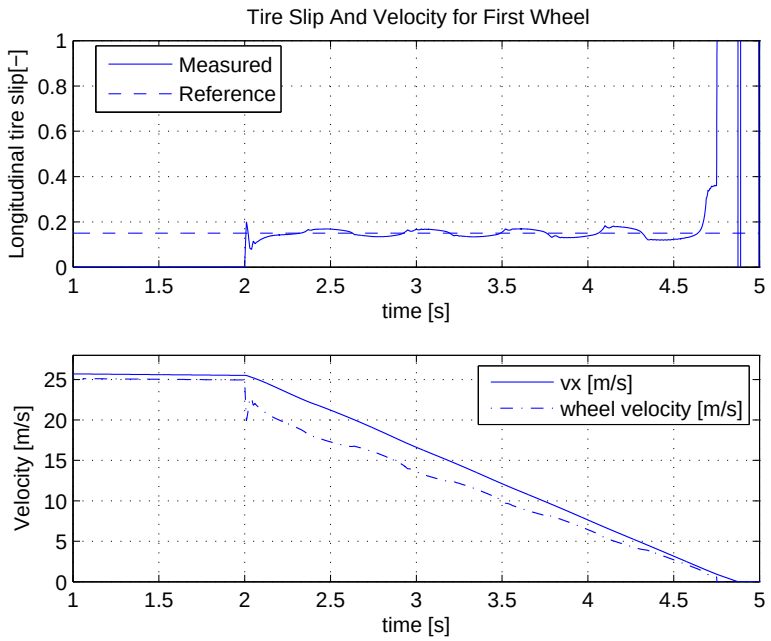

Figure B.1 Tire slip, denoted 'measured', and longitudinal velocity during an ABS braking with $\mu = 1$ and a reference slip of 0.15. The ABS is activated when the slip due to emergency braking goes above some given threshold, in this case $\lambda = 0.15$.

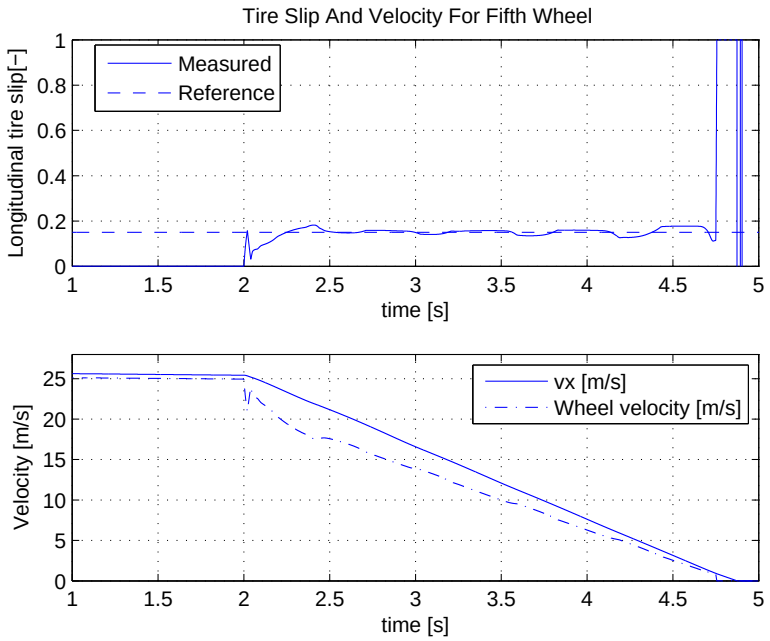

Figure B.2 Tire slip and longitudinal velocity during an ABS braking with $\mu = 1$ and a reference slip of 0.15.

Emergency Braking for $\mu = 0.3$

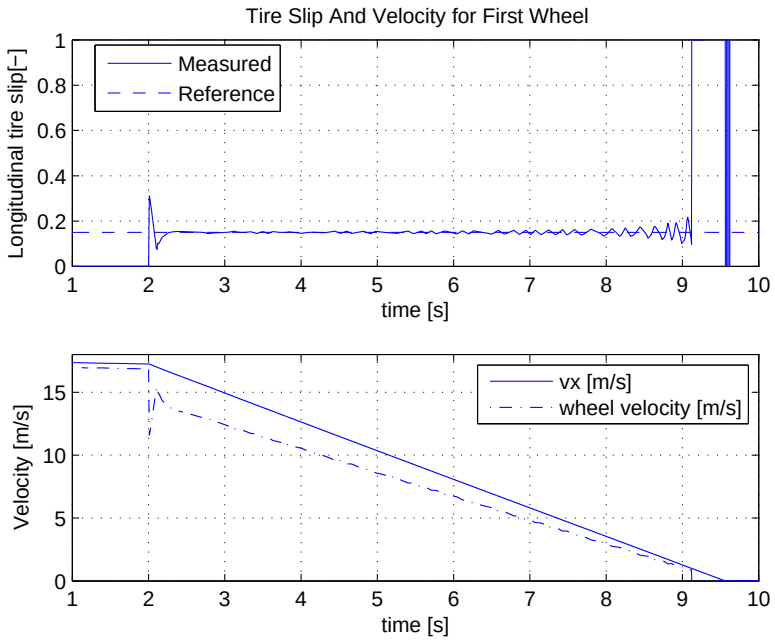

Figure B.3 Tire slip and longitudinal velocity during an ABS braking with $\mu = 0.3$.

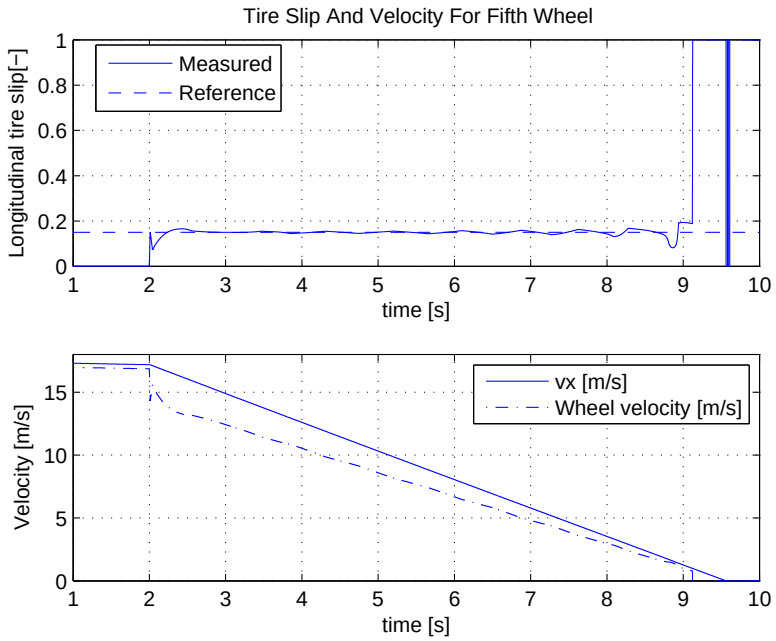

Figure B.4 Tire slip and longitudinal velocity during an ABS braking with $\mu = 0.3$.

μ-Step Braking

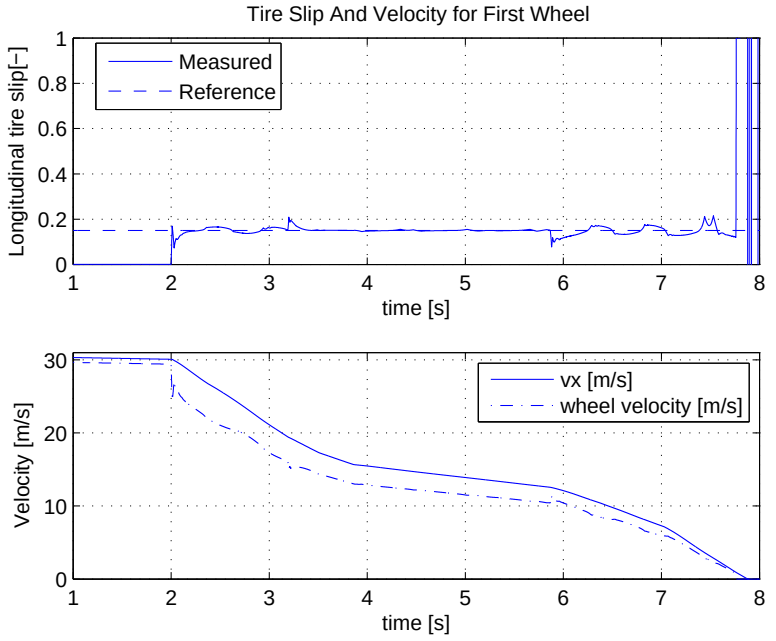

Figure B.5 Tire slip and longitudinal velocity during an ABS μ-step braking and a reference slip of 0.15.

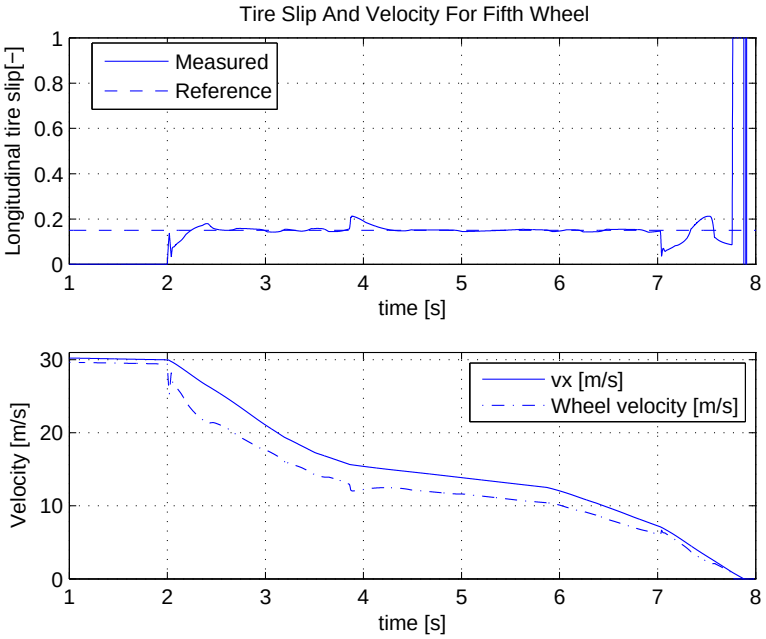

Figure B.6 Tire slip and longitudinal velocity during an ABS μ-step braking.